Relativistic features and time delay of laser-induced tunnel-ionization

Enderalp Yakaboylu, Michael Klaiber, Heiko Bauke, Karen Z. Hatsagortsyan, and Christoph H. Keitel

Max-Planck-Institut für Kernphysik, Saupfercheckweg 1, 69117 Heidelberg, Germany

(Dated: September 4, 2013)

The electron dynamics in the classically forbidden region during relativistic tunnel-ionization process is investigated. The classical forbidden region in the relativistic regime is identified by defining a gauge invariant total energy operator. Introducing position dependent energy levels inside the tunneling barrier, we demonstrate that the relativistic tunnel-ionization can be well described by a one-dimensional intuitive picture. This picture predicts that, in contrast to the well-known nonrelativisitic regime, the ionized electron wave packet in the relativistic regime arises with a momentum shift along the laser propagation direction. This is compatible with results from a strong field approximation calculation where the binding potential is assumed to be zero-range. Further, the tunneling time delay, stemming from Wigner's definition, is investigated for model configurations of tunneling and compared with results obtained from the exact propagator. By adapting Wigner's time delay definition the tunneling time is investigated in the deep-tunneling and in the near-threshold-tunneling regimes. It is shown that while in the deep-tunneling regime signatures of the tunneling time delay are not measurable at remote distance, it is detectable, however, in the latter regime.

I. INTRODUCTION

The investigation of relativistic regimes of laser-atom interactions, in particular the strong field ionization of highly charged ions [1–8], is feasible with current laser technology [9, 10]. Strong field multiphoton atomic processes in the relativistic domain are governed by three parameters [11] which can be chosen to be the Keldysh parameter $\gamma = \omega \sqrt{2I_p}/E_0$ [12], the barrier suppression parameter E_0/E_a and the relativistic laser field parameter $\xi = E_0/(c\omega)$, with the ionization potential I_p, the atomic field $E_a = (2I_p)^{3/2}$, the laser's electric field amplitude E_0, the angular frequency ω and the speed of light c (atomic units are used throughout). At small Keldysh parameters ($\gamma \ll 1$) the laser field can be treated as quasistatic and the ionization is in the so-called tunneling regime up to intensities with $E_0/E_a \lesssim 1/10$, while for higher intensities over-the-barrier ionization dominates [13]. In the nonrelativistic case, the quasistatic tunnel-ionization is a well-established mechanism which is incorporated as a first step in the well-known simple-man three-step model of strong field multiphoton ionization [14]. In the first step of this intuitive picture the bound electron tunnels out through the effective potential barrier governed by the atomic potential $V(\boldsymbol{x})$ and the scalar potential of the quasistatic laser field as $V_{\text{barrier}}(\boldsymbol{x}) = \boldsymbol{x} \cdot \boldsymbol{E}(t_0) + V(\boldsymbol{x})$, where t_0 indicates the moment of the quasistatic tunneling. In nonrelativistic settings, the effect of the magnetic field component of the laser field is neglected and the quasistatic laser field is described solely in terms of the scalar potential $V_{\text{barrier}}(\boldsymbol{x})$. In the second step the ionized electron propagates in the continuum according to the quasiclassical theory and the third step is a potential recollision of the laser driven electron with the ionic core that will not be considered in this manuscript.

When entering the relativistic regime at $\xi^2 \gtrsim 1$, however, the laser's magnetic field modifies the second step via an induced drift motion of the continuum electron into the laser propagation direction. For even stronger laser fields, that is when $I_p/c^2 \sim \gamma^2 \xi^2 \sim 1$, the laser's magnetic field can also not be neglected anymore during the first step. Here, the description

by a sole scalar potential $V_{\text{barrier}}(\boldsymbol{x})$ is not valid anymore and the intuitive picture of tunneling fails. The presence of a vector potential which generates the associated magnetic field leads to a controversy over the effective potential barrier [15]. Hence we ask, can the tunneling picture be remedied for the application in the relativistic regime and can it be formulated in a gauge-independent form? These questions are addressed in this paper and it is shown that for a quasistatic electromagnetic wave, it is possible to define a total energy operator where the tunneling barrier can be identified without any ambiguity in any gauge.

A further interesting and controversial aspect of tunneling and hence tunnel-ionization is the issue of whether the motion of the particle under the barrier is instantaneous or not. The question of whether the tunneling phenomenon confronts special theory of relativity has been raised [16]. The main difficulty in the definition of the tunneling time delay is due to the lack of a well-defined time operator in quantum mechanics. For the generic problem of the tunneling time [17] different definitions have been proposed and the discussion of their relevance still continues [18–25]. Recent interest to this problem has been renewed by a unique opportunity offered by attosecond angular streaking techniques for measuring the tunneling time during laser-induced tunnel-ionization [26–29]. Here we investigate the tunneling time problem for ionization in nonrelativisitic as well as in relativistic settings. For tunnel-ionization by electromagnetic fields there is a direct relationship of the tunneling time to the shift in coordinate space of the ionized electron wave packet in the laser propagation direction at the appearance in the continuum [30]. Within the quasiclassical description, using either the Wentzel-Kramers-Brillouin (WKB) approximation or a path integration in the Euclidean space-time along the imaginary time axis [31–35], the under-the-barrier motion is instantaneous. Thus, we address the time delay problem by going beyond the quasiclassical description. In the present paper, we adopt Wigner's approach to the tunneling time [18–20] which, in simple terms, allows to follow the peak of the tunneled wave packet. We find conditions when a non-vanishing Wigner time delay under the barrier for the

tunnel-ionization is expected to be measurable by attosecond angular streaking techniques.

One of the theoretical tools applied in this paper is the relativistic strong field approximation (SFA) [36, 37]. Neglecting the atomic potential for the continuum electron and approximating its dynamics with the Volkov state is the main approximation of the SFA [12, 38, 39]. Consequently, the prediction of the SFA is much more accurate for a zero-range potential than for a more realistic long-range potential as the Coulomb potential. SFA calculations for the tunnel-ionization modeled with a zero-range potential show that there is a momentum shift along the laser propagation direction due to the tunneling step. We find that this shift can also be estimated via a WKB analysis when a Coulomb potential is used and that it is measurable in a detector after the laser field has been turned off.

The structure of the paper is the following. In Sec. II the parameter domain of the relativistic tunneling dynamics is estimated. In Sec. III the gauge invariance in classical and quantum mechanics is discussed and the gauge independence of the tunneling barrier is established both in nonrelativistic as well as in relativistic settings. The intuitive picture for the tunnel-ionization is discussed in Sec. IV reducing the full problem to an one-dimensional one. In Sec. V the SFA formalism is presented and the momentum distribution at the tunnel exit is calculated. In Sec. VI the tunneling time delay and its corresponding quasiclassical counterpart are investigated and in Sec. VII it is applied to the tunnel-ionization problem. Our conclusions and further remarks are given in Sec. VIII.

II. RELATIVISTIC PARAMETERS

Let us estimate the role of relativistic effects in the tunnel-ionization regime $\gamma \ll 1$. As opposed to the nonrelativistic regime where the typical velocity of the bound electron $\kappa \equiv \sqrt{2I_p}$ is much smaller than the speed of light c and the magnetic force is smaller than the electric force by at least an order of κ/c, we reach relativistic tunnel-ionization when the bound electron approaches velocities of the order of the speed of light and we can not neglect the magnetic field. The tunneling dynamics starts from a bound state with energy I_p, thus the parameter I_p/c^2 identifies the relativistic signature of the initial state, where c^2 is the rest energy. Note that $I_p/c^2 = 1 - \sqrt{1 - (\kappa/c)^2}$ equals 0.01 for the ion charge $\kappa = 20$ and 0.25 for $\kappa = 90$. Furthermore, the influence of the magnetic-dipole correction term can be estimated as being proportional to $(\mathcal{L}B_0/c)/I_p \sim I_p/c^2$, where $\mathcal{L} \sim \Delta z \kappa$ is the typical angular momentum, $\Delta z \sim F_L \tau_K^2$ is the typical distance along the laser propagation direction due to the Lorentz-force $F_L \sim (\kappa/c)B_0$ induced by the laser's magnetic field B_0, and $\tau_K = \gamma/\omega$ denotes the typical ionization time (Keldysh time). Electric as well as magnetic non-dipole terms are negligible since the typical width of the electron's wave packet is small compared to the laser's wavelength $\omega \Delta z/c \sim \gamma I_p/c^2 \ll 1$. Finally, the spin-magnetic field coupling strength E_0/c and spin-orbit coupling $F_C p_z/c^2 \sim \kappa^5/c^3$ with the Coulomb-force $F_C \sim \kappa^3$ and the typical transversal momentum $p_z \sim F_L \tau_k$

are small compared with I_p, see [40, 41], and, therefore, spin effects will be neglected.

In summary, the magnitude of the relativistic effects for the electron dynamics in the classically forbidden region is determined by the parameter $I_p/c^2 = 1 - \sqrt{1 - (\kappa/c)^2}$. They begin to play a role at about $\kappa > 20$, while tunneling does not become fully-relativistic for any atomic species, since I_p/c^2 never reaches the vicinity of one. For this reason, the tunneling dynamics is satisfactory described using an expansion of the Hamiltonian in $1/c$ up to second order, i. e., considering only the magnetic dipole and the mass correction terms [30]. Further, the laser field in the tunneling regime is bounded above via $\sqrt{2I_p/c^2} \ll \xi < \xi_{\text{OTBI}}$, where $\xi_{\text{OTBI}} = (I_p/c^2)^2[c^3/(4\omega\kappa)]$ characterizes the border to over-the-barrier ionization [13]. In the following, we use two extreme but feasible sets of parameters which fulfill the above mentioned physical constraints: $I_p/c^2 = 0.25$ and $E_0/E_a = 1/30$ for the deep-tunneling regime and $E_0/E_a = 1/17$ for the near-threshold-tunneling regime. In the latter we experience a large tunneling probability near the threshold to the over-the-barrier regime.

III. ELECTRODYNAMICS, GAUGE FREEDOM, AND TUNNELING

In this section we demonstrate how the tunneling barrier in the presence of electromagnetic fields can be defined in a gauge invariant manner. For this purpose, we briefly summarize the gauge theory in the light of [42, 43].

A. Gauge theory

In classical electrodynamics the Maxwell equations allow to express the physical quantities, the electric and magnetic fields, in terms of a scalar potential ϕ and a vector potential $\boldsymbol{A}$

$$\boldsymbol{E} = -\nabla\phi - \frac{1}{c}\partial_t\boldsymbol{A}\,, \tag{1}$$

$$\boldsymbol{B} = \nabla \times \boldsymbol{A}\,. \tag{2}$$

Gauge invariance is the feature of electrodynamics that any other pair of a scalar and a vector potential that is related by a so-called gauge transformation describes the same electromagnetic fields. More precisely, the transformation

$$\phi \rightarrow \phi' = \phi - \frac{1}{c}\partial_t\chi\,, \tag{3a}$$

$$\boldsymbol{A} \rightarrow \boldsymbol{A}' = \boldsymbol{A} + \nabla\chi \tag{3b}$$

induced via the gauge function χ leaves the electric field and the magnetic field invariant. Consequently, all physically measurable electrodynamic quantities, the Maxwell equations, and the Lorentz force law are gauge invariant. This means they do not depend on the choice for the electromagnetic potentials. Furthermore, the Schrödinger equation for a particle in electromagnetic fields is invariant under the transformation (3) provided that the state vector transforms with the gauge transformation $U = \exp(-i\chi/c)$ as

$$|\psi\rangle \rightarrow U|\psi\rangle\,. \tag{4}$$

B. Gauge invariant energy operator

Besides the elegance of the gauge theory, all the physical quantities, i. e., the experimental observables cannot depend on the choice of the gauge function. Let us discuss if a physical tunneling potential barrier can be defined in a gauge independent manner.

Each physical operator that corresponds to a measurable quantity must be gauge independent. For example, the canonical momentum operator $\boldsymbol{p}$, transforms under the gauge transformation U as

$$\boldsymbol{p} \to U\boldsymbol{p}U^{\dagger} = \boldsymbol{p} + \frac{1}{c}\nabla\chi \neq \boldsymbol{p}\,. \tag{5}$$

The kinetic momentum $\boldsymbol{q}(\boldsymbol{A}) = \boldsymbol{p} + \boldsymbol{A}/c$, however, obeys

$$\boldsymbol{q}(\boldsymbol{A}) \to U\boldsymbol{q}U^{\dagger} = \boldsymbol{p} + \boldsymbol{A}'/c = \boldsymbol{q}(\boldsymbol{A}')\,. \tag{6}$$

Here, the canonical momentum $\boldsymbol{p}$ which generates the space translation and satisfies the canonical commutation relation is not a physical measurable quantity, it is the kinetic momentum $\boldsymbol{q}(\boldsymbol{A})$ that is measured in the experiment. In general, any operator that satisfies the transformation

$$O(\boldsymbol{p}, \boldsymbol{x}, \boldsymbol{A}, \phi) \to UO(\boldsymbol{p}, \boldsymbol{x}, \boldsymbol{A}, \phi)U^{\dagger} = O(\boldsymbol{p}, \boldsymbol{x}, \boldsymbol{A}', \phi') \tag{7}$$

is called as a physical operator. For instance, the Hamiltonian for a charge particle interacting with an arbitrary electromagnetic field in the nonrelativisitic regime

$$H = \frac{(\boldsymbol{p} + \boldsymbol{A}/c)^2}{2} - \phi \tag{8}$$

transforms under the gauge transformation as

$$H \to \frac{(\boldsymbol{p} + \boldsymbol{A}'/c)^2}{2} - \phi\,. \tag{9}$$

Hence, it cannot be a physical operator (because ϕ is not equally transformed to ϕ'), while $H - i\partial/\partial t$ is the physical operator which guarantees the invariance of the Schrödinger equation under a gauge transformation.

In contrast to the Hamiltonian H, the total energy of a system has to be a gauge invariant physical quantity. Therefore, we have to distinguish two concepts: the Hamiltonian and the total energy. The Hamiltonian is the generator of the time translation, while the total energy is defined as a conserved quantity of the dynamical system under a time translation symmetry of the Lagrangian. As a consequence, if the Hamiltonian is explicitly time independent, then the Hamiltonian coincides with the total energy operator.

For a time independent electromagnetic field there exists a certain gauge where the Hamiltonian is explicitly time independent. The identification of the Hamiltonian as a total energy operator implies, then, that both the vector potential $\boldsymbol{A}$ and the scalar potential ϕ associated to the constant electromagnetic field have to be time independent. This leads to the fact that

$$\phi = -\int^{\boldsymbol{x}} \boldsymbol{E}(\boldsymbol{x}') \cdot d\boldsymbol{x}' \tag{10}$$

where we have used Eq. (1). In this gauge, the Hamiltonian which coincides with the total energy operator $\hat{\varepsilon}$ in the presence of any external potential $V(\boldsymbol{x})$ reads

$$H = \hat{\varepsilon} = \frac{(\boldsymbol{p} + \boldsymbol{A}(\boldsymbol{x})/c)^2}{2} + \int^{\boldsymbol{x}} \boldsymbol{E}(\boldsymbol{x}') \cdot d\boldsymbol{x}' + V(\boldsymbol{x})\,, \tag{11}$$

where the time independent vector potential $\boldsymbol{A}(\boldsymbol{x})$ generates the associated magnetic field via Eq. (2).

Accordingly, if we identify Eq. (11) as a definition of the gauge independent total energy operator, it reads in an arbitrary gauge

$$\hat{\varepsilon} = \frac{(\boldsymbol{p} + \boldsymbol{A}(\boldsymbol{x}, t)/c)^2}{2} + \int^{\boldsymbol{x}} \boldsymbol{E}(\boldsymbol{x}') \cdot d\boldsymbol{x}' + V(\boldsymbol{x})\,, \tag{12}$$

where we have used the transformation (7). The first term on the right hand side of (12) is the kinetic energy for an arbitrary vector potential $\boldsymbol{A}(\boldsymbol{x}, t)$ that appears in the corresponding Hamiltonian. The second term should not be regarded as a scalar potential, but defines the potential energy. The energy operator (12) fulfills the conservation law

$$\frac{d\hat{\varepsilon}}{dt} = i[H, \hat{\varepsilon}] + \frac{\partial\hat{\varepsilon}}{\partial t} = 0\,, \tag{13}$$

which can be prooven in a straightforward calculation. We find

$$\frac{\partial\hat{\varepsilon}}{\partial t} = \frac{1}{2}\left((\boldsymbol{p} + \boldsymbol{A}/c) \cdot \frac{\partial\boldsymbol{A}}{c\partial t} + \frac{\partial\boldsymbol{A}}{c\partial t} \cdot (\boldsymbol{p} + \boldsymbol{A}/c)\right)\,, \tag{14}$$

$$[H, \hat{\varepsilon}] = \frac{1}{2}\left((\boldsymbol{p} + \boldsymbol{A}/c) \cdot \left[\boldsymbol{p}, \int^{\boldsymbol{x}} \boldsymbol{E} \cdot d\boldsymbol{x}' + \phi\right] + \left[\boldsymbol{p}, \int^{\boldsymbol{x}} \boldsymbol{E} \cdot d\boldsymbol{x}' + \phi\right] \cdot (\boldsymbol{p} + \boldsymbol{A}/c)\right) \tag{15}$$

and hence

$$\frac{d\hat{\varepsilon}}{dt} = \frac{1}{2}\left(\left(\boldsymbol{p} + \frac{\boldsymbol{A}}{c}\right) \cdot \left(\boldsymbol{E} + \nabla\phi + \frac{\partial\boldsymbol{A}}{c\partial t}\right) + \left(\boldsymbol{E} + \nabla\phi + \frac{\partial\boldsymbol{A}}{c\partial t}\right) \cdot \left(\boldsymbol{p} + \frac{\boldsymbol{A}}{c}\right)\right) = 0 \tag{16}$$

is obtained. The definition (12), then, suggests to introduce the gauge independent effective potential energy as

$$V_{\text{eff}}(\boldsymbol{x}) = \int^{\boldsymbol{x}} \boldsymbol{E}(\boldsymbol{x}') \cdot d\boldsymbol{x}' + V(\boldsymbol{x})\,. \tag{17}$$

In conclusion, the electron dynamics during ionization can be described as tunneling through a potential barrier if the total energy of the electron is conserved. Then, the potential energy and the tunneling barrier can be identified unambiguously. Thus, for ionization in a laser field we have to identify the quasistatic limit such that the tunneling picture becomes applicable. The tunnel-ionization regime in a laser field is determined by the Keldysh parameter $\gamma \ll 1$. It defines the so-called tunneling formation time $\tau_K = \gamma/\omega$, see Sec. V C. The tunneling regime $\gamma \ll 1$ corresponds to situations when the formation time of the ionization process is much smaller than the laser period. Consequently, the electromagnetic field

can be treated as quasi-static during the tunneling ionization process and the electron energy is approximately conserved. Therefore, the gauge-independent operator for the total energy $\hat{\varepsilon}$ in a quasistatic electromagnetic field can be defined and from the latter the gauge-independent potential energy can be deduced, which in the case of tunnel-ionization constitutes the gauge-independent tunneling barrier. Therefore, Eq. (17) defines the gauge independent tunneling barrier in the tunnel-ionization regime. In the long wavelength approximation it yields

$$V_{\text{barrier}} = \boldsymbol{x} \cdot \boldsymbol{E}(t_0) + V(\boldsymbol{x}), \tag{18}$$

where t_0 is the moment of ionization and $V(\boldsymbol{x})$ is the binding potential for the tunnel-ionization.

As an illustration of the gauge independence of the tunneling barrier, let us compare two fundamental gauges used in strong field physics to describe nonrelativistic ionization. In the length gauge where $\phi = -\boldsymbol{x} \cdot \boldsymbol{E}_0$, $\boldsymbol{A} = 0$, the nonrelativistic Hamiltonian for a constant uniform electric field is given by

$$H = \frac{\boldsymbol{p}^2}{2} + \boldsymbol{x} \cdot \boldsymbol{E}_0 + V(\boldsymbol{x}). \tag{19}$$

Here, the Hamiltonian coincides to the physical energy operator. In the velocity gauge, however, where $\boldsymbol{A} = -c\boldsymbol{E}_0 t$, $\phi = 0$, the same dynamics is governed by the Hamiltonian

$$H = \frac{(\boldsymbol{p} - \boldsymbol{E}_0 t)^2}{2} + V(\boldsymbol{x}). \tag{20}$$

In Eq. (20) it seems as if there is no potential barrier. However, the *conserved* energy operator

$$\hat{\varepsilon} = \frac{(\boldsymbol{p} - \boldsymbol{E}_0 t)^2}{2} + \boldsymbol{x} \cdot \boldsymbol{E}_0 + V(\boldsymbol{x}), \tag{21}$$

reveals the tunneling barrier $\boldsymbol{x} \cdot \boldsymbol{E}_0 + V(\boldsymbol{x})$. Thus, for arbitrary time independent (quasistatic) electromagnetic fields, the gauge-independent tunneling barrier can be defined without any ambiguity.

The physical energy operator and the tunneling barrier can be generalized to the relativistic regime straightforwardly by using the relativistic Dirac Hamiltonian

$$H = c\boldsymbol{\alpha} \cdot (\boldsymbol{p} + \boldsymbol{A}/c) - \phi + V(\boldsymbol{x}) + \beta c^2. \tag{22}$$

From Eq. (12) we deduce the physical energy operator in the relativistic case as

$$\hat{\varepsilon} = c\boldsymbol{\alpha} \cdot (\boldsymbol{p} + \boldsymbol{A}(\boldsymbol{x}, t)/c) + \int^{\boldsymbol{x}} \boldsymbol{E}(\boldsymbol{x}') \cdot d\boldsymbol{x}' + V(\boldsymbol{x}) + \beta c^2. \tag{23}$$

One possible generalization of the length gauge into the relativistic regime is the Göppert-Mayer gauge

$$A^\mu = -\boldsymbol{x} \cdot \boldsymbol{E}(\eta)(1, \hat{\boldsymbol{k}}), \tag{24}$$

where the phase of the electromagnetic wave is given by $\eta = x^\mu k_\mu = \omega(t - \hat{\boldsymbol{k}} \cdot \boldsymbol{x}/c)$, $x^\mu = (c\,t, \boldsymbol{x})$, and $k^\mu = \omega/c(1, \hat{\boldsymbol{k}})$ with the propagation direction $\hat{\boldsymbol{k}}$. Taking into account that the dipole approximation for the laser field can be applied inside the
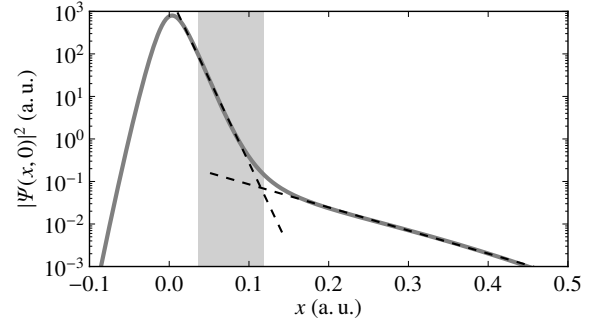

FIG. 1. The electron density (solid line) along the laser polarization direction at the instant of maximal field strength at the atomic core. The shaded area represents the classical forbidden area, gray dashed lines are exponential fits on the wave function density. The electron's wave function $\Psi(x, z)$ is obtained by solving the two-dimensional Dirac equation for an electron in a soft-core potential interacting with an external laser pulse, laser parameters are the same as in [30].

tunneling barrier, the Hamiltonian which coincides with the total relativistic energy operator in the Göppert-Mayer gauge reads

$$H = \hat{\varepsilon} = c\boldsymbol{\alpha} \cdot \left(\boldsymbol{p} - \hat{\boldsymbol{k}} \frac{\boldsymbol{x} \cdot \boldsymbol{E}(\eta_0)}{c} \right) + \boldsymbol{x} \cdot \boldsymbol{E}(\eta_0) + V(\boldsymbol{x}), \tag{25}$$

where η_0 is the laser phase at the moment of ionization.

The tunneling barrier results from an interpretation of the individual mathematical terms of the quasistatic energy operator (25). It has, however, also a physical significance as it can be demonstrated by an ab initio numerical simulation of the tunneling process in a highly charged ion in a laser field of relativistic intensities based on the Dirac equation [30, 44]. Figure 1 shows the gauge-independent electron density along the laser polarization direction at the instant of maximal field strength at the atomic core. The electron density can be divided in two parts that are characterized by two different decay rates. The switchover region includes the tunneling exit that is defined by the tunneling barrier. The decay of the density under the barrier is related to damping due to tunneling, i. e., approximately $\sim \exp(-\kappa x)$, whereas outside the barrier it is dominated by transversal spreading. As the change of slopes occurs close to the tunneling exit the tunneling barrier is real and physical and not just a result of an interpretation in a particular gauge.

IV. INTUITIVE PICTURE FOR THE RELATIVISTIC TUNNEL-IONIZATION PROCESS

Having identified the gauge invariant tunneling barrier, we elaborate in this section on the intuitive picture for the tunnel-ionization process in the relativistic regime. For the reminder of the article we choose our coordinate system such that the laser's electric field component $\boldsymbol{E}_0$ is along the x direction, the laser's magnetic component $\boldsymbol{B}_0$ is along the y direction and the laser propagates along the z direction. Since we assume to work in the quasistatic regime, the Göppert-Mayer gauge Hamiltonian is used that coincides with the energy operator. In
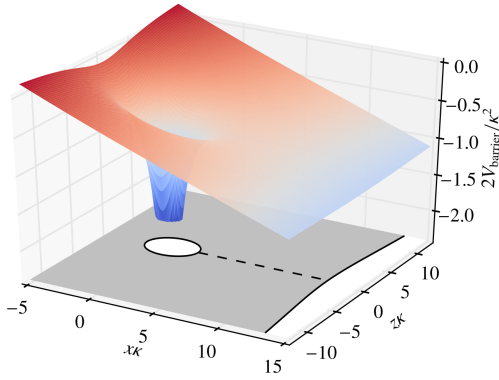
FIG. 2. (Color online) The potential barrier V_{barrier} for quasistatic tunnel-ionization with no magnetic field in the plane of the direction of the electric field and the laser's propagation direction. The laser field $E(t_0) = -\kappa^3/30$ is along the x direction. The most probable tunneling path is indicated by the black dashed line.

the nonrelativistic limit the latter equals the Göppert-Mayer-Schrödinger Hamiltonian while in the fully relativistic regime the Göppert-Mayer-Dirac Hamiltonian will be applied.

A. Nonrelativistic case

In the nonrelativistic limit the intuitive picture for the tunnel-ionization is well-known. In this picture the magnetic field and nondipole effects can be neglected, and the Hamiltonian reads

$$H = \frac{\boldsymbol{p}^2}{2} + xE(t_0) - \frac{\kappa}{r}, \tag{26}$$

with $r = \sqrt{x^2 + y^2 + z^2}$. Introducing the potential

$$V_{\text{barrier}}(\boldsymbol{x}) = xE(t_0) - \frac{\kappa}{r}, \tag{27}$$

one can define the classical forbidden region. The tunneling probability increases with decreasing width of the barrier, thus, the most probable tunneling path is concentrated along the electric field direction as indicated by the dashed line in Fig. 2. Therefore, it is justified to restrict the analysis of the tunneling dynamics along the laser's polarization direction [45].

In this one-dimensional picture the barrier for the tunnel-ionization follows as

$$V_{\text{barrier}} = xE(t_0) - \frac{\kappa}{|x|}. \tag{28}$$

The momentum components p_y and p_z along the y and the z direction are conserved and tunneling along the x direction is governed by the energy

$$\varepsilon_x = -I_p - \frac{p_y^2}{2} - \frac{p_z^2}{2}. \tag{29}$$

The wave function of the electron and the corresponding transition probability can be derived within the Wentzel-Kramers-Brillouin (WKB) approximation. The zeroth order WKB wave function is given by

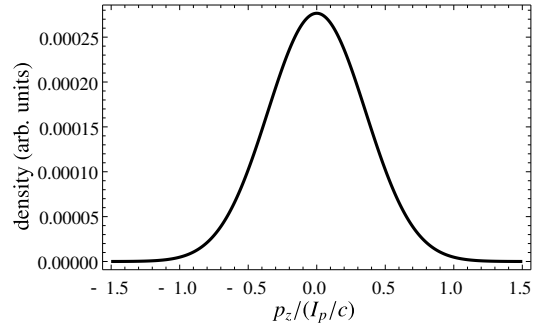$$\psi \propto \exp\left(iS_{cl}\right), \tag{30}$$

FIG. 3. The nonrelativistic tunneling probability versus the momentum along z direction. The maximum tunneling probability occurs at $p_z = 0$. The applied parameters are $E(t_0) = -\kappa^3/30$ and $\kappa = 90$. Without loss of generality, $p_y = 0$ was chosen.

with the classical action

$$S_{\text{cl}} = -\varepsilon_x t + \int^x p_x(x')\,dx', \tag{31}$$

and the momentum's x component

$$p_x(x) = \sqrt{2(\varepsilon_x - V_{\text{barrier}})}. \tag{32}$$

The WKB tunneling probability follows as

$$|T|^2 \propto \exp\left(-2\int_{x_0}^{x_e} dx\,|p_x(x)|\right), \tag{33}$$

where x_0 and x_e are the entry point and exit point of the barrier such that $p(x_0) = p(x_e) = 0$. The dependence of the tunneling probability on the momentum p_z is shown Fig. 3. The tunneling probability is maximal for $p_z = 0$, because the energy level (29) decreases with increasing p_z^2. From this it follows that the exit coordinate increases with increasing p_z.

In summary, nonrelativistic tunneling from an atomic potential can be visualized by an one-dimensional picture given in Fig. 4(a) and (b). The area between the barrier and the energy level represents a messure for the probability of the process. The larger the area the less likely the ionization.

B. Relativistic case

In the relativistic regime, the largest correction to the nonrelativistic Hamiltonian comes from the magnetic dipole term. Let us consider the role of the magnetic dipole interaction in the laser field for the tunneling picture. The corresponding time-independent Schrödinger equation reads

$$\left[\frac{(-i\nabla - xE(t_0)\hat{z}/c)^2}{2} + xE(t_0) - \frac{\kappa}{r}\right]\psi(\boldsymbol{x}) = \varepsilon\,\psi(\boldsymbol{x}). \tag{34}$$

Similar to the nonrelativistic case, an approximate one-dimensional description is valid for the most probable tunneling path along the electric field direction. Restricting the dynamics around the electric field direction and neglecting the dependence of ionic core's potential on the transverse coordinate, we have $p_{y,z} = \text{const}$, and the momentum along the
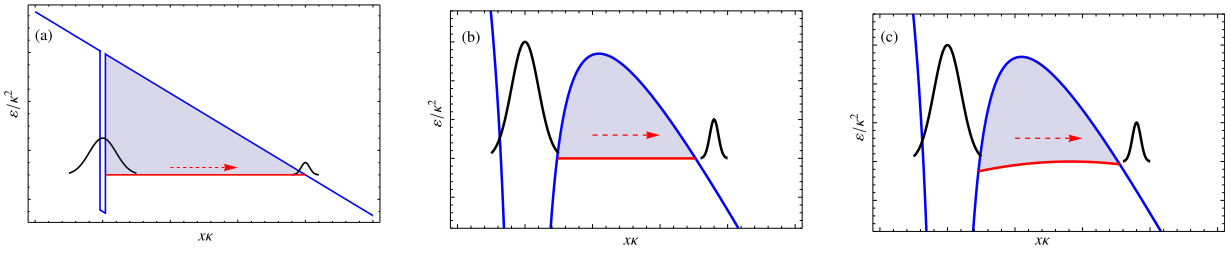
FIG. 4. (Color online) Schematic picture of nonrelativistic (sub-figures (a) and (b)) and relativistic (subfigure (c)) tunneling from a bound state into the continuum: (a) the atomic potential is aproximated by a zero-range potential; (b) and (c) the Coulomb potential case. The potential barrier (solid, blue) and the energy levels (dashed, red) for $p_z = 0$ (in the nonrelativistic cases) and for the most probable transversal momentum p_z (relativistic case) are plotted against the longitudinal tunneling coordinate x. The shaded area can be interpreted as a measure for the tunneling probability. The electron wave packet is indicated in black.

polarization direction is given by Eq. (32) with the barrier (28), which is the same as in the nonrelativistic case. The energy, however, is modified by the magnetic dipole term

$$\varepsilon_x = -I_p - \frac{p_y^2}{2} - \frac{(p_z - xE(t_0)/c)^2}{2}. \qquad (35)$$

The energy level (35) depends on the x coordinate. This is because the electron's kinetic momentum along the laser's propagation direction $q_z(x) \equiv p_z - xE(t_0)/c$ changes during tunneling due to the presence of the vector potential (magnetic field). As a consequence, the tunneling probability in the relativistic regime is maximal at some non-zero canonical momentum p_z in the laser's propagation direction. For instance, the kinetic momentum $q_z(x)$ with maximal tunneling probability at the tunneling entry is $q_z(x_0) \approx -0.42 I_p/c$, whereas at the exit it is $q_z(x_e) \approx 0.28 I_p/c$ for the Coulomb potential, see Fig. 5. During the under-the-barrier motion the electron acquires a momentum kick into the laser's propagation direction due to the Lorentz force, which can be estimated as

$$\Delta p_z \sim x_e E_0/c \sim I_p/c, \qquad (36)$$

with the barrier length $x_e \sim I_p/E_0$. Thus, relativistic tunneling can be visualized by an one-dimensional picture given in Fig. 4(c). The area between the barrier and the position dependent energy level is larger than in the nonrelativistic case due to the non-vanishing transversal kinetic energy, indicating the reduced tunneling probability in the relativistic description.

The WKB analysis can be carried out also in a fully relativistic way. Taking into account the relativistic energy-momentum dispersion relation, one obtains for the momentum and the ionization energy along the polarization direction

$$\varepsilon_x = \sqrt{p_x^2 c^2 + c^4} + V_{\text{barrier}} - c^2, \qquad (37)$$

$$p_x(x) = \sqrt{\left(\frac{c^2 - I_p - V_{\text{barrier}}}{c}\right)^2 - c^2 - p_y^2 - \left(p_z - \frac{xE(t_0)}{c}\right)^2} \qquad (38)$$

which determines the fully relativistic tunneling probability via Eq. (33). The latter is shown in Fig. 5. For comparison it shows also the results for the nonrelativistic case, the calculation using

the magnetic dipole correction, and the calculation with the leading relativistic kinetic energy correction $-\hat{p}_x^4/8c^2$ [46].

As demonstrated in Fig. 5 the shift of the kinetic momentum along the laser propagation direction that maximizes the WKB tunneling probability is determined mainly by the magnetic dipole correction to the Hamiltonian. This correction also decreases the tunneling probability, since the Lorentz force due to the laser's transversal magnetic field transfers energy from the tunneling direction into the perpendicular direction hindering tunneling. Taking into account further relativistic effects does not change the behavior qualitatively but increases the tunneling probability. This can be understood intuitively by noticing that in the reference frame of the relativistic electron the length of the barrier is contracted and in this way enhancing the tunneling probability. The mass correction term is more important in the zero-range-potential case than in the Coulomb-potential one, since the typical longitudinal velocities are smaller in the latter case. Furthermore, Fig. 5 indicates that the calculation including only the leading relativistic kinetic energy correction $O(1/c^2)$ reproduces the fully-relativistic approach satisfactorily. Thus, the magnetic dipole and the leading order mass shift are the only relevant relativistic corrections.

The value of the kinetic momentum shift at tunnel exit $q_z(x_e)$ varies significantly with respect to the barrier suppression parameter E_0/E_a in the case of a Coulomb potential of the ionic core, as shown in Fig. 6, while it does not depend on the laser field in the case of zero-range atomic potential. The main reason for the decreased momentum shift in the Coulomb potential case is that the length of the Coulomb-potential barrier is reduced by a factor $\approx (1 - 8E_0/E_a)$ compared to the barrier length of the zero-range potential. According to Eq. (36), this barrier length reduction leads to smaller momentum kick due to the magnetic field.

Furthermore, we compare the prediction of the WKB approximation with the results obtained by an *ab initio* numerical calculation solving the time-dependent Dirac equation [44]. For this purpose the tunnel-ionization from a two-dimensional soft-core potential was simulated yielding the time-dependent real space wave function $\Psi(x, z, t)$. A transformation into a mixed representation of position x and kinetic momentum q_z via

$$\tilde{\Psi}(x, q_z, t) = \frac{1}{\sqrt{2\pi}} \int \Psi(x, z, t) e^{-iz(q_z - A_z(x,z))} dz \qquad (39)$$
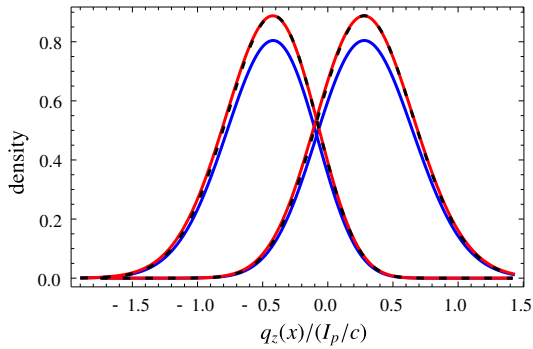
FIG. 5. (Color online) Tunneling probability vs. the kinetic momentum along the laser propagation direction at the tunnel entry (lines with peak on the left) and tunnel exit (lines with peak on the right). Results for calculations including magnetic dipole correction are indicated in blue while for the red lines also the leading relativistic correction to the kinetic energy are taken into account. The dashed-black lines correspond to a fully relativistic calculation, which are very close to the ones including leading relativistic corrections to the kinetic energy. The densities are normalized to the maximum density in the nonrelativisitic case. A similar comparison was made in [30] for the case of a zero-range potential via SFA.
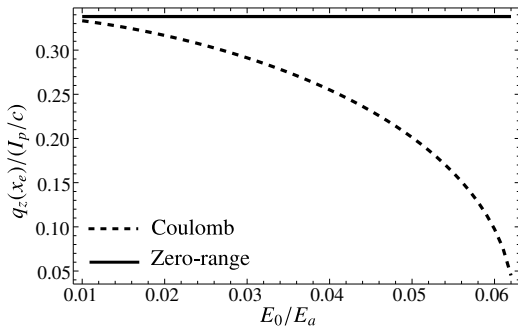
FIG. 6. The kinetic momentum shift at the tunnel exit $q_z(x_e)$ versus the barrier suppression parameter E_0/E_a for an electron bound by a Coulomb potential (dashed) and a zero-range atomic potential (solid).

allows us to determine the kinetic momentum in z direction as a function of the x coordinate and in this way at the tunnel exit $x = x_e$, see Fig. 7. Both, the solution of the fully relativistic Dirac equation and the WKB approximation predict a momentum distribution with a maximum shifted away from zero. The momentum shifts are in a good agreement.

V. TUNNEL-IONIZATION WITH A ZERO-RANGE POTENTIAL MODEL

The intuitive considerations of the previous section on the relativistic under-the-barrier motion during tunnel-ionization led us to the conclusion that relativistic tunneling induces a momentum kick along the laser's propagation direction. The aim of this section to prove this conclusion by a rigorous calculation based on SFA, to show how this momentum shift arises during the under-the-barrier motion, and to find out how this
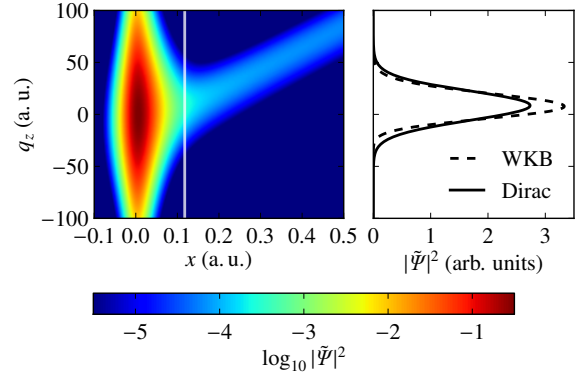

FIG. 7. (Color online) Electronic density in the mixed space of position x and kinetic momentum q_z at the moment of maximal field strength at the atomic core (left panel). The electron's wave function has been obtained by simulating the tunnel-ionization from a two-dimensional soft-core potential by solving the time-dependent Dirac equation with all numerical parameters as in Fig. 1. The right panel shows the normalized kinetic momentum distribution of the tunneled electron at the tunnel exit (indicated by the white line in the left panel) as obtained by solving the Dirac equation and by the WKB approximation.

relativistic signature is reflected in the electron momentum distribution in far distance at the detector.

The SFA is based on an S-matrix formalism. The ionization is described by the Hamiltonian

$$H = H_0 + H_I(t), \qquad (40)$$

where H_0 is the field-free atomic Hamiltonian including the atomic potential $V(x)$ and $H_I(t)$ denotes the Hamiltonian of the laser-atom interaction. Initially at time $t \to -\infty$, the electron is in the bound state $|\psi(-\infty)\rangle = |\phi_0\rangle$. In SFA the influence of atomic core potential on the free electron and the influence of the laser field on the bound state are neglected. This allows us to express the time evolution of the state vector in the form [11]

$$|\psi(t)\rangle = -i \int_{-\infty}^{t} dt' \, U_V(t, t') H_I(t') |\phi_0(t')\rangle, \qquad (41)$$

where $U_V(t, t')$ is the Volkov propagator which satisfies

$$i \frac{\partial U_V(t, t')}{\partial t} = H_V(t) U_V(t, t') \qquad (42)$$

with the Volkov Hamiltonian $H_V = H - V(x)$. The SFA wave function in momentum space of the final state reads

$$\langle p|\psi\rangle = -i \int_{-\infty}^{\infty} dt' \, \langle \psi_V(t')|H_I(t')|\phi_0(t')\rangle, \qquad (43)$$

where $|\psi_V(t)\rangle$ denotes a Volkov state [47]. The ionized part of the wave function in momentum space in Eq. (43) can be expressed also in the form [11]

$$\langle p|\psi\rangle = -i \int_{-\infty}^{\infty} dt' \, \langle \psi_V(t')| V(x) |\phi_0(t')\rangle. \qquad (44)$$

As the SFA neglects the effect of the atomic potential on the final state, the SFA gives an accurate prediction when the atomic potential is short ranged. For this reason, we will model the tunnel-ionization with a zero-range potential in the following. The nonrelativistic tunneling scheme for this case is visulized in Fig. 4(a). The barrier has triangular shape which simplifies the analytical treatment of the tunneling dynamics.

A. Nonrelativistic case

Let us start our analysis with the nonrelativistic consideration when the Hamiltonian for an atom in a laser field is given by Eq. (40) with

$$H_0 = \frac{p^2}{2} + V^{(0)}(\mathbf{x}), \tag{45}$$

$$H_I = \mathbf{x} \cdot \mathbf{E}(t), \tag{46}$$

where $V^{(0)}(\mathbf{x})$ is the zero-range atomic potential. In SFA the ionized part of the wave function far away after the laser field has been turned off reads [41]

$$\langle \mathbf{p}|\psi\rangle = -i\mathcal{N} \int_{-\infty}^{\infty} dt\, e^{-i\tilde{S}(\mathbf{p},t)}, \tag{47}$$

where $\tilde{S}(\mathbf{p},t) = -\kappa^2 t/2 - \int^t dt'\, \mathbf{q}^2/2$ is the contracted action, $\mathbf{q} = \mathbf{p} + \mathbf{A}/c$ is the kinetic momentum, $\mathbf{A} = -c\int^t \mathbf{E}\,dt'$, $\mathcal{N} \equiv \langle \mathbf{q}|V^{(0)}|\phi^{(0)}\rangle = \text{const}$, and $|\phi^{(0)}\rangle e^{i\kappa^2 t/2}$ is the bound state of the zero-range potential. The time integral in Eq. (47) can be calculated via the saddle point approximation (SPA). The saddle point equation

$$\dot{\tilde{S}}(\mathbf{p},t_s) = \mathbf{q}(t_s)^2 + \kappa^2 = 0 \tag{48}$$

yields the kinetic momentum $\mathbf{q}(t_s) = i\kappa$ at the saddle point time t_s. Then, the wave function in momentum space reads in the quasi-static limit

$$\langle \mathbf{p}|\psi\rangle = -i\mathcal{N} \sqrt{\frac{2\pi}{|E(t_s)|\sqrt{p_\perp^2 + \kappa^2}}} \exp\left[-\frac{(p_\perp^2 + \kappa^2)^{3/2}}{3|E(t_s)|}\right] \tag{49}$$

for the vector potential $\mathbf{A} = cE_0 \sin(\omega t)/\omega \hat{\mathbf{x}}$ and with $E(t_s) = \left|E_0\sqrt{1 - (p_x/(E_0/\omega))^2}\right|$ and $p_\perp = \sqrt{p_y^2 + p_z^2}$. From expression (49) it follows that the density of the ionized wave function is maximal at $p_\perp = 0$ for any value of p_x. The coordinate space wave function

$$\langle \mathbf{x}|\psi\rangle = -i\frac{\mathcal{N}}{(2\pi)^{3/2}} \int_{-\infty}^{\infty} dt \int d^3p\, \exp\left[i\mathbf{x}\cdot\mathbf{p} - i\tilde{S}(\mathbf{p},t)\right] \tag{50}$$

is obtained by a Fourier transform of Eq. (47). From the SPA it follows that the main contribution to the integral over $\mathbf{p}$ in Eq. (50) originates from momenta near the momentum which fulfills the saddle point condition $\mathbf{x} - \partial_{\mathbf{p}}\tilde{S}(\mathbf{p},t) = 0$. The latter defines the trajectories $\mathbf{x} = \mathbf{x}(\mathbf{p},t)$ which contribute to the transition probability with amplitudes depending on $\mathbf{p}$. For the
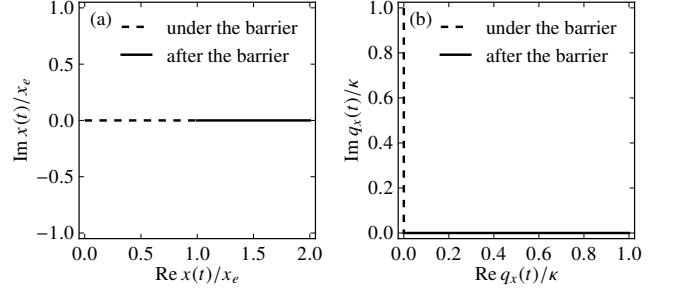

FIG. 8. Coordinate (sub-figure (a)) and momentum (sub-figure (b)) along the laser field direction of the complex SFA trajectory for tunnel-ionization from a zero-range potential. During the under-the-barrier motion the momentum is imaginary whereas the coordinate is real. Tunneling finishes when the kinetic momentum becomes real.

most probable final momentum $\mathbf{p}_0 = 0$, the trajectory which start at the tunneling entry at time t_s is given by

$$\mathbf{x}(t) = \partial_{\mathbf{p}}\tilde{S}(\mathbf{p}_0, t) = \int_{t_s}^{t} dt'\, \frac{\mathbf{A}(t')}{c}. \tag{51}$$

The line integral in Eq. (51) is along a path connecting the complex time t_s with the real time t. The complex saddle point time t_s can be determined by solving $q(t_s) = i\kappa$ for t_s. The corresponding kinetic momentum is

$$\mathbf{q}(t) = \frac{\mathbf{A}(t)}{c}. \tag{52}$$

In Fig. 8 the complex trajectory (51) and the complex kinetic momentum (52) along the tunneling direction are shown. The spatial coordinate is real under the barrier as well as behind the barrier, whereas the kinetic momentum is imaginary during tunneling and becomes real when leaving the barrier, which corresponds to the time $\text{Re}(t_s)$. The tunneling exit coordinate is $x_e = x_e(\text{Re}\{t_s\}) = I_p/E_0$ which is consistent with the intuitive tunneling picture. The momentum in the tunneling direction is $q(t_s) = i\kappa$ when tunneling starts, whereas it is $q(\text{Re}\{t_s\}) = 0$ at the tunnel exit.

B. Relativistic case

Our fully relativistic consideration is based on the Dirac Hamiltonian with a zero-range atomic potential

$$H = c\boldsymbol{\alpha} \cdot (\mathbf{p} + \mathbf{A}/c) - \phi + \beta c^2 + V^{(0)}(\mathbf{x}) \tag{53}$$

where $\boldsymbol{\alpha}$ and β are standard Dirac matrices [48] and the Göppert-Mayer gauge (24) is employed. The ionized part of the momentum wave function in SFA yields

$$\langle \mathbf{p}|\psi\rangle = -i \int_{-\infty}^{\infty} dt \int d^3x\, \overline{\psi}_V(\mathbf{x},t)\gamma^0 V^{(0)}(\mathbf{x})\phi^{(0)}(\mathbf{x},t). \tag{54}$$

Here $\phi^{(0)}(\mathbf{x},t) = e^{-i\varepsilon_0 t}\varphi^{(0)}(\mathbf{x})v^{(0)}_\pm$ is the ground state of the zero-range potential with the ground state spinor $v^{(0)}_\pm$ and

$\varepsilon_0 = c^2 - I_p$; $\psi_V(\boldsymbol{x}, t) = N_V u_\pm e^{iS}$ is the relativistic Volkov wave function in the Göppert-Mayer gauge for a free electron in a laser field, which is obtained from the Volkov function in the velocity gauge [47] with further gauge transformation via the gauge function $\chi = -\boldsymbol{x} \cdot \boldsymbol{A}/c$, $\boldsymbol{A}(\eta) \equiv -\frac{c}{\omega} \int^\eta \boldsymbol{E}(\eta')d\eta'$. Furthermore, N_V is the normalization constant,

$$S = -\varepsilon t + \left(\boldsymbol{p} + \frac{\boldsymbol{A}}{c}\right) \cdot \boldsymbol{x} - \frac{1}{c\Lambda} \int^\eta \left(\boldsymbol{p} \cdot \boldsymbol{A} + \frac{\boldsymbol{A}^2}{2c}\right) d\eta', \quad (55)$$

is the quasiclassical action and

$$u_\pm = \left(1 + \frac{\omega}{2c^2\Lambda}(1 + \boldsymbol{\alpha} \cdot \hat{\boldsymbol{k}})\boldsymbol{\alpha} \cdot \boldsymbol{A}\right) u_{0\pm}, \quad (56)$$

with $\Lambda = p^\mu k_\mu = \omega(\varepsilon/c^2 - \boldsymbol{p} \cdot \hat{\boldsymbol{k}}/c)$, $p^\mu = (\varepsilon/c, \boldsymbol{p})$, and the free particle spinor $u_{0\pm}$. After averaging over the spin of the initial electron as well as over the spin of the ionized electron the wave function of the ionized electron reads

$$\langle \boldsymbol{p}|\psi \rangle = -i\frac{N_V(2\pi)^{3/2}}{2\omega} \int_{-\infty}^{\infty} d\eta \, e^{-i\tilde{S}} \sum_{s,s'} \langle \boldsymbol{q}_d, s'| V^{(0)}(\boldsymbol{x}) |\varphi_0, s \rangle . \quad (57)$$

Here, a coordinate transformation $(t, \boldsymbol{x}) \rightarrow (\eta, \boldsymbol{x})$ is employed and

$$\tilde{S} = \frac{1}{2\Lambda} \left(-\kappa^2 \eta - \int^\eta \boldsymbol{q}_d^2 d\eta'\right) \quad (58)$$

is the contracted action with the field-dressed electron momentum in the laser field

$$\boldsymbol{q}_d = \boldsymbol{p} + \frac{\boldsymbol{A}}{c} - \frac{\hat{\boldsymbol{k}}(\varepsilon - \varepsilon_0)}{c} . \quad (59)$$

For a zero-range potential the inner product $\langle \boldsymbol{q}_d, s'| V^{(0)}(\boldsymbol{x}) |\varphi_0, s \rangle$ is only η dependent. Further, the η-integral in (55) can be calculated using SPA and the saddle point equation yields $\boldsymbol{q}_d^2(\eta_s) = -\kappa^2$ as in the nonrelativistic regime [49]. Then, the wave function of the ionized electron in momentum space yields

$$\langle \boldsymbol{p}|\psi \rangle = -i\mathcal{N}(\eta_s) \sqrt{\frac{2\pi\Lambda}{\omega E(\eta_s) \sqrt{q_{d\perp}^2 + \kappa^2}}} \exp\left[-\frac{\omega(q_{d\perp}^2 + \kappa^2)^{3/2}}{3\Lambda E(\eta_s)}\right] \quad (60)$$

for the vector potential $\boldsymbol{A} = cE_0 \sin(\eta)/\omega \hat{\boldsymbol{x}}$ with the laser's propagation vector $\hat{\boldsymbol{k}} = \hat{\boldsymbol{z}}$, where

$$E(\eta_s) = \left|E_0 \sqrt{1 - (p_x/(E_0/\omega))^2}\right|, \quad (61)$$

$$q_{d\perp} = \sqrt{p_y^2 + \left(p_z - \frac{\varepsilon - \varepsilon_0}{c}\right)^2}, \quad (62)$$

$$\mathcal{N}(\eta_s) = \frac{N_V(2\pi)^{3/2}}{2\omega} \sum_{s,s'} \langle \boldsymbol{q}, s'| V^{(0)}(\boldsymbol{x}) |\varphi_0, s \rangle . \quad (63)$$

The relativistic momentum distribution of the ionized electron of Eq. (60) differs qualitatively from the nonrelativistic one. In the nonrelativistic case the maximum of the distribution is at $p_\perp = 0$ at any p_x. In the relativistic case, however, the
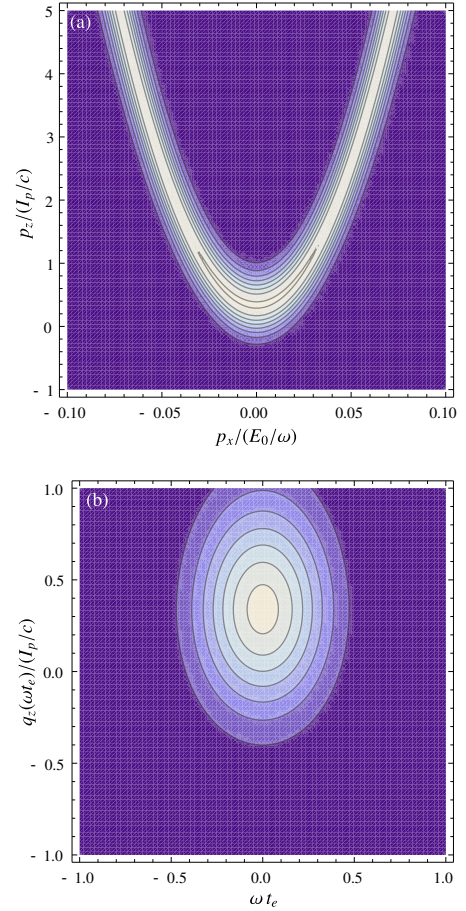

FIG. 9. (Color online) The momentum distribution of the ionized electron: (a) in infinity at the detector; (b) at the tunnel exit, depending on the tunnel exit time t_e. The maximum tunneling probability occurs at $p_z = I_p/(3c)$. The applied parameters are $\kappa = 90$, $E_0/E_a = 1/30$ and $\omega = 10$.

momentum distribution has a local maxima along the parabola which can be approximated as

$$p_z \approx \frac{I_p}{3c}\left(1 + \frac{I_p}{18c^2}\right) + \frac{p_x^2}{2c}\left(1 + \frac{I_p}{3c^2} + \frac{2I_p^2}{27c^4}\right) + O\left(\frac{I_p^2}{c^4}\right), \quad (64)$$

see Fig. 9(a). The global maximum of the tunneling probability is located at $p_z = I_p/(3c)$, while in the nonrelativistic case it is at $p_z = 0$. This shift of the maximum is connected with the first step of the ionization, the tunneling, whereas the parabolic wings are shaped in the second step, the continuum dynamics. These wings are located around $p_z = U_p/c$.

The momentum distribution at the tunnel exit can be calculated via back propagation of the final momentum space wave function (60). Thus, the wave function at the tunnel exit is

$$\langle \boldsymbol{p}|\psi(t_e) \rangle = \int d^3p' \langle \boldsymbol{p}| U(t_e, t_f) |\boldsymbol{p}' \rangle \langle \boldsymbol{p}'|\psi(t_f) \rangle$$

$$\approx \int d^3p' \langle \boldsymbol{p}| U_V(t_e, t_f) |\boldsymbol{p}' \rangle \langle \boldsymbol{p}'|\psi(t_f) \rangle \quad (65)$$

with the tunnel exit time $t_e = \text{Re}(t_s)$ and final time t_f where the interaction is turned off, hence the Volkov wave function

reduces to the free particle wave function. Because $\omega \hat{\boldsymbol{k}} \cdot \boldsymbol{x} \ll c$ holds at the tunnel exit holds, the exact Volkov propagator

$$\langle \boldsymbol{x}| U_V(t,t')|\boldsymbol{x}'\rangle = \int d^3p \; \psi_V(t,\boldsymbol{x})\psi_V^\dagger(t',\boldsymbol{x}') \qquad (66)$$

can be simplified expanding the phase dependent functions around ωt_e, which yields

$$U_V(t_e,t_f) = \int d^3p \; \exp\left(i\varphi(t_e,t_f)\right)|\boldsymbol{p}_e\rangle \langle \boldsymbol{p}| \qquad (67)$$

with the exit momentum and the phase

$$\boldsymbol{p}_e = \boldsymbol{p} + \frac{\boldsymbol{A}(\omega t_e)}{c} + \hat{\boldsymbol{k}}\frac{\omega}{c^2\Lambda}(\boldsymbol{p} + \frac{\boldsymbol{A}(\omega t_e)}{2c}) \cdot \boldsymbol{A}(\omega t_e)\,, \quad (68)$$

$$\varphi(t_e,t_f) = \varepsilon(t_f - t_e) + \frac{1}{c\Lambda}\int^{\omega t_e} d\eta \left(\boldsymbol{p} + \frac{\boldsymbol{A}(\eta)}{2c}\right)\cdot \boldsymbol{A}(\eta)\,, \quad (69)$$

respectively. As a result, the momentum space wave function at the tunnel exit t_e reads in terms of the final wave function $\langle \boldsymbol{p}'|\psi(t_f)\rangle$

$$\langle \boldsymbol{p}|\psi(t_e)\rangle = e^{i\varphi(t_e,t_f)}\langle \boldsymbol{p}'|\psi(t_f)\rangle \qquad (70)$$

with

$$\boldsymbol{p}' = \left(-\frac{A_x(\omega t_e)}{c}, p_y, p_z + \frac{A_x(\omega t_e)^2\omega}{2c^3\Lambda}\right)\,. \qquad (71)$$

The transversal momentum distribution at the tunnel exit can be calculated via replacing the momentums in the wave function Eq. (60) with Eq. (71), which can be seen in Fig. 9(b). The comparison of Figs. 9(a) and (b) indicates that the relativistic shift of the peak of the transverse momentum distribution at the tunnel exit $p_z = I_p/(3c)$ is maintained in the final momentum distribution. The parabola can for example be calculated from classical trajectories. The kinetic momentum at the exit is connected with the final momenta via

$$q_x(\eta_s) = p_x + \frac{A(\eta_s)}{c} = 0\,,$$

$$q_z(\eta_s) = p_z + \frac{\omega}{c^2\Lambda}\left(p_x A(\eta_s) + \frac{A(\eta_s)^2}{2c}\right) = \frac{I_p}{3c} \qquad (72)$$

and the relation

$$p_z = \frac{I_p}{3c} + \frac{\omega p_x^2}{2c\Lambda} \qquad (73)$$

follows.

We investigate the trajectory of the electron and its momentum during the tunneling in the relativistic regime. The coordinate wave function can be obtained via a Fourier transform of momentum space wave function (57). Then, the stationary phase condition gives the quasiclassical trajectories at the most probable momentum given by Eq. (64). The results are plotted in Fig. 10. It shows that in the relativistic regime most probable trajectory is the trajectory where the electron enters the barrier with the transversal momentum $-2I_p/(3c)$ and reaches the exit with $I_p/(3c)$. This is in accordance with our intuitive discussion in Sec. IV.
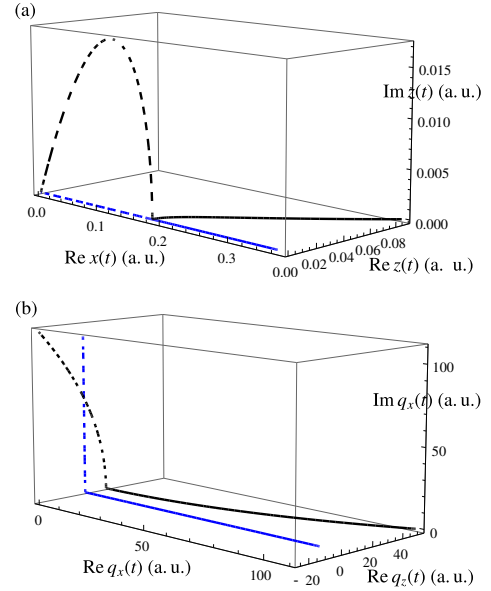
FIG. 10. (Color online) Comparison of the nonrelativisitic (blue) and relativistic (black) complex SFA trajectories: (a) coordinates and (b) momentum components. The dashed and the solid lines correspond to the under-the-barrier motion and the motion after the tunneling, respectively. In the relativistic regime, the trajectory enters the tunneling barrier at $(0,0)$, it is complex under the barrier and becomes real again when it leaves the tunneling barrier. The trajectory enters the barrier with the transversal momentum $-2I_p/(3c)$ and leaves the barrier with $I_p/(3c)$. The applied parameters are $\kappa = 90$, $E_0/E_a = 1/30$.

For the most probable momentum, the trajectory starts at the real axis, obtains complex values during tunneling and has to return to the real axis after tunneling Fig. 10(a). Here an analogy to relativistic high-harmonic generation can be drawn, where also a return condition has to be fulfilled: the recollision of the ionized electron to the atomic core in the presence of the drift motion induced by the laser's magnetic field [50]. Similarly, the electron has to start with a momentum of the order of U_p/c against the laser propagation direction (cf. $q_{z,i} = -2I_p/(3c)$ at the entering the ionization barrier) which compensates the drift motion and facilitates the recollision to the atomic core with a momentum U_p/c along the laser propagation direction (cf. $q_{z,e} = I_p/(3c)$ at the exit of the ionization barrier).

The shift of the electron's momentum distribution along the laser's propagation direction in the relativistic regime is possible to detect by measuring the final momentum distribution of the ion [51]. The ionized electron acquires momentum along the laser's propagation direction in the laser field because of the absorbed momentum of the laser photons. However, part of the momentum of laser photons is transferred to the ion. The energy conservation law provides a relationship between the number of absorbed photons n and the electron momentum p_e

$$n\omega - I_p + c^2 \approx \varepsilon_e\,, \qquad (74)$$

where ω is the laser frequency, I_p the ionization potential, and $\varepsilon_e = c\sqrt{p_e^2 + c^2}$ the energy of the electron. The kinetic energy
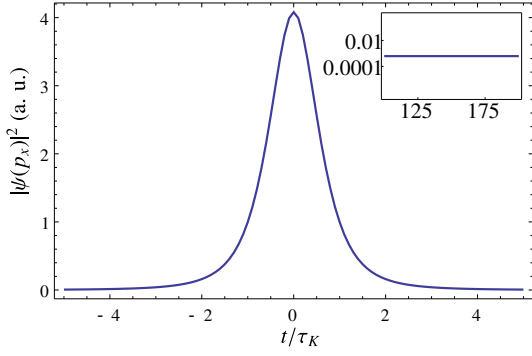
FIG. 11. The ionization momentum amplitude for $p_x = 0$ vs. the observation time t. The inset shows the momentum amplitude for large times, which coincides with the ionization amplitude.

of the ionic core can be neglected due to the large mass of the ion. Additionally, the momentum conservation law gives information on the sharing of the absorbed photon momentum between the ion and the photoelectron

$$\begin{pmatrix} n\omega/c \\ 0 \\ 0 \end{pmatrix} = \begin{pmatrix} p_{ez} + p_{0z} \\ p_{ex} + p_{0x} \\ p_{ey} + p_{0y} \end{pmatrix}. \qquad (75)$$

In the nonrelativisitic tunneling regime of ionization in the linearly polarized laser field, the photoelectron's most probable momentum is $p_e = 0$, when $n\omega = I_p$ and the ion carries out a momentum $p_{0z} = I_p/c$. In the relativistic regime of interaction the most probable value of the photoelectron's momentum is not vanishing but equals $p_{ez} \approx I_p/3c$ in the case of linear polarization. In this case the momentum conservation will provide the ion momentum $p_{0z} \approx 2I_p/3c$. In [51, 52] the momentum sharing between ion and electron during the tunnel-ionization in a strong circularly polarized laser field is investigated. Their result supports the simple-man model prediction. It is shown that the total momentum of the absorbed photons, that is I_p/c, is transferred to the ion and not to the ionized electron. The difference with respect to our result may be explained by the focal averaging as well as by the fact that our parameters are situated in the pure tunneling regime whereas the references deal with ionization at the transition to over-the-barrier ionization. The momentum shift of the ionized electrons at the detector that we describe is a genuine feature of the relativistic tunneling dynamics.

C. Tunneling formation time

The physical interpretation of the Keldysh time as the ionization formation time given in Sec. III B can be readily clarified within the SFA formalism. In SFA the momentum wavefunction at some intermediate time is given by

$$\langle p_x|\psi \rangle \sim \int_\infty^t dt' \exp[iS(t,t')] \qquad (76)$$

with the quasiclassical action $S(t,t') = \int_{t'}^t d\tilde{t}(p_x + A(\tilde{t})^2/2 + I_p t'$. A numerical integration of the integral in Eq. (76) shows that

the value of the momentum amplitude starts with zero at early times then varies on a time scale that is of the order of the Keldysh time, see Fig. 11. Thus, the Keldysh time is the typical time scale for the formation of the moment components of the ionized wave function, or in short, the formation time of the ionization. Finally, the momentum amplitude stabilizes on the positive value which can be identified as the ionization amplitude of the specific momentum component, see inset in Fig. 11.

VI. GENERAL ASPECTS OF TUNNELING TIME DELAY

In quantum mechanics time as it stands is a parameter and not an observable. Furthermore, as it is discussed by Pauli [53, 54], it can not be upgraded to an operator which is conjugate to the Hamiltonian. It is due to the fact that although the time can take any values, the spectrum of allowed energy levels of a given Hamiltonian can not span the entire real line. Namely, either the Hamiltonian is bounded below or it may take discrete values due to the quantization conditions. Nevertheless, a time delay problem can be formulated in quantum mechanics. It is possible to put forward in a reasonable way within quantum mechanics the question on how much time an electron spends in a specified space region during its motion and, in particular, what is the time delay for the tunneling through a potential barrier [17–22, 25, 55–57]. Several definitions for the time delay have been proposed, one of the most accepted definitions is the Eisenbud-Wigner-Smith time delay (here refered to as the Wigner time delay.) [18–20].

The definition of the Wigner time delay is based on the trajectory of the peak of the electron wave packet, as long as the wave packet has a unique peak. Let us illustrate it considering the motion of the following wave packet in the position space

$$\langle x|\psi(t) \rangle = \frac{1}{\sqrt{2\pi}} \int_{-\infty}^\infty dp \exp(ipx) \langle p|\psi(t) \rangle, \qquad (77)$$

assuming that the wave packet in momentum space $\langle p|\psi(t) \rangle$ is centered around p_0 and is expressed in the form

$$\langle p|\psi(t) \rangle = g(p) \exp(-i\phi(p,t)), \qquad (78)$$

with real functions g and ϕ. The peak of the wave packet in position space at a moment t

$$\langle x|\psi(t) \rangle = \frac{1}{\sqrt{2\pi}} \int_{-\infty}^\infty dp \exp(i(px - \phi(p,t))) g(p) \qquad (79)$$

can be found in the limit $\Delta p_g \gg \phi'(p_0)$, with the width Δp_g of the density g, by the stationary phase approximation, and is given by the stationary phase condition

$$\frac{\partial}{\partial p}(px - \phi(p,t))\bigg|_{p_0} = 0 \quad \Rightarrow \quad x = \frac{\partial\phi(p,t)}{\partial p}\bigg|_{p_0}. \qquad (80)$$

In the limit $\Delta p_g \ll \phi'(p_0)$, the phase ϕ can be linearized, viz., $\phi(p) = \phi(p_0) + \phi'(p_0)(p - p_0)$ and the maximum of the wave-packet is shifted from 0 to $\phi'(p_0)$ due to the additional

coordinate translation operator $\exp\left[ip\phi'(p_0)\right]$. Therefore, in both cases the phase derivative at p_0 yields the coordinate of the maximum of the wave-packet. In fact, this result is consistent with the expectation value of the position operator

$$\langle x \rangle = \langle \psi(t)| x |\psi(t)\rangle = \int_{-\infty}^{\infty} dp \left(ig(p)g(p)' + g(p)^2\phi(p,t)'\right). \tag{81}$$

In the latter, the first term vanishes because the wave packet is initially formed symmetrically around p_0, while from the second term one has $\langle x \rangle \approx \phi(p_0,t)'$, if the phase $\phi(p,t)'$ is expanded around p_0 and the third and higher-order derivatives are neglected.

Similarly, the wave packet in position space can be expanded in energy eigenfunctions with energy eigenvalues ε [58]

$$\langle x|\psi(t)\rangle = \int_0^{\infty} d\varepsilon \, \langle x|\varepsilon \rangle \langle \varepsilon|\psi(t)\rangle$$
$$= \int_0^{\infty} d\varepsilon \, f(x,\varepsilon) \exp\left(i\varphi(x,\varepsilon) - i\varepsilon(t-t_0)\right), \tag{82}$$

where $f(x,\varepsilon) \equiv \langle \varepsilon|\psi(t_0)\rangle \,|\,\langle x|\varepsilon\rangle|$ and $\langle \varepsilon|\psi(t_0)\rangle$ is the energy distribution of initial wave packet at $t = t_0$ which is symmetrically centered around ε_0, and $\varphi(x,\varepsilon)$ is the phase of $\langle x|\varepsilon\rangle$ which is the steady-state solution. Analogously to the dicussion on the coordinate maximum, the condition

$$\tau \equiv t - t_0 = \left.\frac{\partial\varphi(x,\varepsilon)}{\partial\varepsilon}\right|_{\varepsilon_0}, \tag{83}$$

then determines the moment when the wave packet is maximal at a given point with coordinate x, i. e. , the Wigner trajectory. Equation (83) indicates that the phase of the steady state solution to the Schrödinger equation is sufficient to deduce the Wigner trajectory. The difference between the Wigner trajectory and the classical trajectory (no time interval is spent under the barrier and the trajectory obeys Newton's law outside the barrier) at points far behind the barrier we call Wigner time delay [19]. In the following we will apply the Wigner time delay formalism to some exactly solvable basic systems under the dynamics of the Schrödinger equation with some potential $V(x)$. These examples will give us some hints for the analysis of tunnel-ionization process.

A. Square potential

As a first example we consider the Wigner time delay during the penetration of a wave packet through a box potential

$$V(x) = V_0 \left(\theta(x) - \theta(x-a)\right) \tag{84}$$

with $\theta(x)$ denoting the Heaviside step function. The wave packet propagating to the barrier and tunneling through it is constructed via superposing the steady-state solutions with energy eigenvalues $\varepsilon < V_0$,

$$\langle x|\psi(t)\rangle = \int_0^{V_0} d\varepsilon \, \exp\left(-i\varepsilon(t-t_0) + i\phi(x,\varepsilon)\right) g(x,\varepsilon) \tag{85}$$

with $g(x,\varepsilon) = \langle \varepsilon|\psi(t_0)\rangle \,|u(x,\varepsilon)|$. Here $\langle \varepsilon|\psi(t_0)\rangle$ is the initial wave packet centered around $\varepsilon_0 < V_0$, $|u(x,\varepsilon)|$ and $\phi(x,\varepsilon)$ are the amplitude and the phase of the steady-state solution $u(x,\varepsilon)$ for $\varepsilon < V_0$, respectively. Generally, the wave packet in Eq. (85) includes both transmitted and reflected waves. To define the Wigner trajectory for the transmitted wave packet, we omit the reflected wave packet from the barrier and utilize the steady-state solutions with the positive current

$$u_+(x,\varepsilon) = \begin{cases} e^{ik_1 x} & x < 0 \\ C_1\left(e^{-k_2 x} + ie^{k_2 x}\right) + C_2\left(e^{-k_2 x} - ie^{k_2 x}\right) & 0 \le x \le a \\ T e^{ik_1 x} & x > a \end{cases} \tag{86}$$

with $k_1 = \sqrt{2\varepsilon}$, $k_2 = \sqrt{2V_0 - 2\varepsilon}$, and the matching coefficients C_1, C_2 and T [59]. The Wigner trajectory for the transmitted wave can then be defined implicitly via

$$\tau(x) = \left.\frac{\partial\varphi_+(x,\varepsilon)}{\partial\varepsilon}\right|_{\varepsilon=\varepsilon_0} \tag{87}$$

where $\varphi_+(x,\varepsilon)$ is the phase of $u_+(x,\varepsilon)$.

The Wigner trajectory for the outgoing wave packet defined in Eq. (87), is shown Fig. 12(a) and is compared with the classical trajectory. From the latter one can see that the Wigner trajectory, which initially coincides with the classical one, deviates during tunneling from the classical trajectory. In the quasiclassical limit $\kappa a \gg 1$, the Wigner time delay is $\tau = 1/2 \sqrt{(V_0 - \epsilon)\epsilon}$ which is formed at the entering and exiting the barrier.

This simple example provides us the opportunity to compare Wigner's approach with the exact trajectory of the wave packet's maximum which can be calculated via Eq. (85). Let us choose the initial normalized wave packet in momentum space as the Gaussian

$$\langle p|\psi(t_0 = 0)\rangle = \frac{e^{-ix_0(p-p_0)}}{(2\pi\delta p^2)^{1/4}} \exp\left[-\left(\frac{p-p_0}{2\delta p}\right)^2\right], \tag{88}$$

with the initial position x_0 and initial momentum $p_0 = \sqrt{2\varepsilon_0}$. The position x_0 is assumed to be far away from the barrier and the energy spread $\delta\varepsilon$ of the wave packed so small that $\varepsilon_0 + \delta\varepsilon < V_0$ with $\delta\varepsilon = p_0\delta p$. To be consistent with the tunnelionization case where the wave packet has a sharp energy we assume that $\delta p/p \ll 1$. Then, the time evolution of the wave packet becomes

$$\langle x|\psi(t)\rangle = \int_0^{\infty} d\varepsilon \, \frac{\langle x|\varepsilon\rangle}{(2\pi\delta p^2)^{1/4}} e^{-i\varepsilon t - ix_0(\sqrt{2\varepsilon} - \sqrt{2\varepsilon_0}) - \left(\frac{\sqrt{2\varepsilon} - \sqrt{2\varepsilon_0}}{2\delta p}\right)^2}. \tag{89}$$

If we trace the maximum of the wave packet outside the barrier, we see that it overlaps with the Wigner's trajectory defined in Eq. (87). The result can be seen in Fig. 12(b).

To evaluate the role of the magnetic field in relativistic tunnel-ionization, we modify the previous configuration by applying an additional static magnetic field within the square potential. The vector potential which generates the magnetic field $\boldsymbol{B} = -E_0\left(\theta(x) - \theta(x-a)\right)\hat{y}$ may be written as

$$\boldsymbol{A} = E_0\left(x\left(\theta(x) - \theta(x-a)\right) + a\theta(x-a)\right)\hat{z}. \tag{90}$$
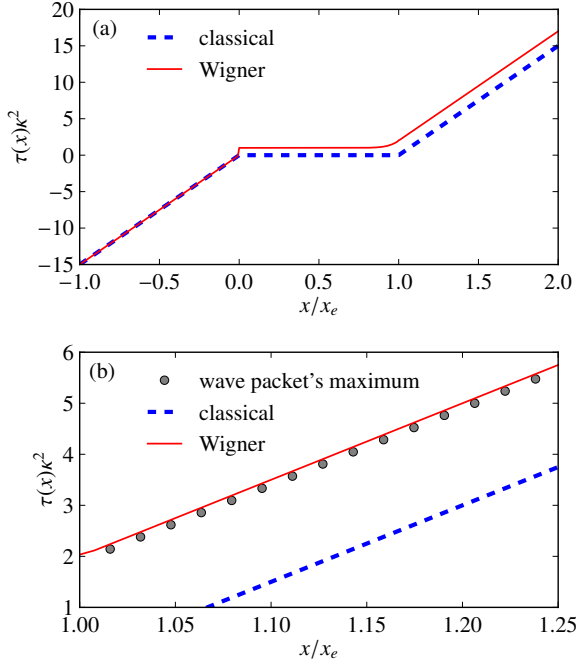
FIG. 12. (Color online) (a) Comparison of the Wigner trajectory (87 (solid red line) and the classical (dashed blue line) trajectory for tunneling through a square potential barrier (84) for $\kappa = 90$ and $a = 15/\kappa$. (b) Close-up of sub-figure (a) with additionally showing the position of the wave packet's maximum.

Then, the Hamiltonian for this field configuration is

$$H = \frac{p_x^2}{2} + \frac{[p_z + A_z(x)/c]^2}{2} + V(x). \qquad (91)$$

Since the canonical momentum p_z is conserved, $[p_z, H] = 0$, the energy eigenfunction has the form

$$\langle x, z|\varepsilon, p_z\rangle = \frac{u(x, p_z, \varepsilon)}{\sqrt{2\pi}} e^{ip_z z}, \qquad (92)$$

and the motion along x coordinate is separable

$$\left[-\frac{1}{2}\frac{d^2}{dx^2} + \frac{(p_z + A_z(x)/c)^2}{2} + V(x) \right] u(x, p_z, \varepsilon) = \varepsilon\, u(x, p_z, \varepsilon). \qquad (93)$$

The solution of Eq. (93) outside the barrier is given by

$$u(x, p_z, \varepsilon) = \begin{cases} u_1(x, p_z, \varepsilon) = e^{ik_1 x} + R e^{-ik_1 x} & x < 0 \\ u_3(x, p_z, \varepsilon) = T e^{ik_3 x} & x > a \end{cases} \qquad (94)$$

with $k_1 = \sqrt{2\varepsilon - p_z^2}$, $k_3 = \sqrt{2\varepsilon - (p_z + aE_0/c)^2}$, and reflection and transmission coefficients are R and T, respectively. For the dynamics under the barrier ($0 \leq x \leq a$, $\varepsilon < V_0$) the Schrödinger equation

$$\left[-\frac{1}{2}\frac{d^2}{dx^2} + \frac{(p_z - xE_0/c)^2}{2} + V_0 \right] u_2(x, p_z, \varepsilon) = \varepsilon\, u_2(x, p_z, \varepsilon). \qquad (95)$$

has two linearly independent solutions which can be expressed using parabolic cylinder function D [60] as

$$u_2(x, p_z, \varepsilon) = C_1\, D\left(-\frac{E_0 + 2cV_0 - 2c\varepsilon}{2E_0}, \frac{\sqrt{2}(cp_z + E_0 x)}{\sqrt{cE_0}} \right)$$
$$+ C_2\, D\left(-\frac{E_0 - 2cV_0 + 2c\varepsilon}{2E_0}, \frac{i\sqrt{2}(cp_z + E_0 x)}{\sqrt{cE_0}} \right). \qquad (96)$$

Here, the matching coefficients C_1 and C_2 can be found via using the continuity of the wave function at the borders of the potential $x = 0$ and $x = a$.

The wave packet tunneling out of the potential barrier is

$$\langle x, z|\psi(t)\rangle = \int_{-\infty}^{\infty} dp_z \int_0^{V_0} d\varepsilon\, \langle x, z|\varepsilon, p_z\rangle \langle \varepsilon, p_z|\psi(t)\rangle$$
$$= \frac{1}{\sqrt{2\pi}} \int_{-\infty}^{\infty} dp_z \int_0^{V_0} d\varepsilon\, e^{izp_z - i\varepsilon(t-t_0) + i\phi_+(x, p_z, \varepsilon)} g(x, p_z, \varepsilon), \qquad (97)$$

where $g(x, p_z, \varepsilon) = \langle \varepsilon, p_z|\psi(t_0)\rangle |u(x, p_z, \varepsilon)|$, $\langle \varepsilon, p_z|\psi(t_0)\rangle$ is the initial wave packet centered around p_{z0} and ε_0, and $\phi_+(x, p_z, \varepsilon)$ is the phase of the outgoing part of $u(x, p_z, \varepsilon)$.

Calculating the transition probability $|T|^2$ as a function of p_z, we find that the maximum is reached at $p_{z0} = -I_p/(2c)$ which equals the kinetic momentum at the tunneling entry $x = 0$, $q_z(0) = -I_p/(2c)$. At the tunneling exit $x = a$ the kinetic momentum with maximal tunneling probability is $q_z(a) = p_{z0} + A_z(a)/c = I_p/(2c)$.

As the phase now depends also on p_z Eq. (87) generalizes to

$$\tau(x) = \left.\frac{\partial\varphi_+(x, p_z, \varepsilon)}{\partial\varepsilon}\right|_{\varepsilon=\varepsilon_0}. \qquad (98)$$

Thus for each choice of p_z Eq. (98) defines a different trajectory and setting $p_z = p_{z0}$ in Eq. (98) gives the most probable trajectory, which is shown in Fig. 13(b) together with the classical one. Comparing Figs. 12(a) and 13(a) shows that presence of the magnetic field does not change the Wigner time delay.

In analogy to Eq. (80), one can also define the coordinate z as a function of x

$$z = -\left.\frac{\partial\phi_+(x, p_z, \varepsilon_0)}{\partial p_z}\right|_{p_z=p_{z0}}, \qquad (99)$$

which gives the most probable trajectory in the x-z-plane as shown in Fig. 13(c) together with the corresponding classical trajectory. Outside the barrier both are close together; under the barrier, however, there is a clear spatial drift into the z-direction, that is perpendicular to the tunneling direction, of the Wigner trajectory as compared to the classical one. Nevertheless, this spatial drift is (in contrast to the Wigner time delay) not observable on the detector at remote distance. This is intuitively plausible, because the drift at the entry point to the barrier $\Delta z_d(0) = q_z(0)\tau = -(I_p/2c)\tau$ is exactly compensated by the drift at the exit point $\Delta z_d(a) = q_z(a)\tau = (I_p/2c)\tau$.
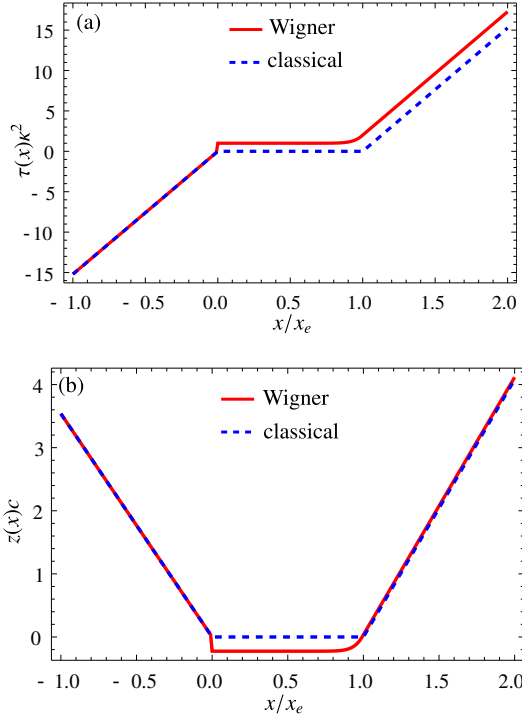
FIG. 13. (Color online) Tunneling through a square potential with an additional magnetic field with $E_0 = \kappa^3/30$ and other parameters as in Fig. 12. Sub-figures (a) and (b) compare the Wigner (red solid lines) and the classical (blue dashed lines) trajectories along the x direction and in the x-z-plane, respectively.
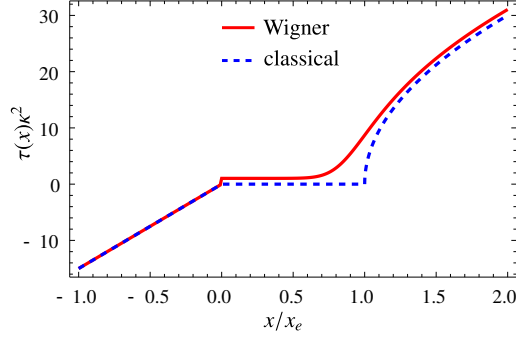

FIG. 14. (Color online) Comparison of the Wigner trajectory (red solid line) and the classical trajectory (blue dashed line) for tunneling through a linear potential barrier (100) for $V_0 = \alpha\varepsilon_0$, $\varepsilon_0 = I_p$, $I_p = c^2 - \sqrt{c^4 - c^2\kappa^2}$, with the numerical parameters $\kappa = 90$, $\alpha = 2$ and $E_0/E_a = 1/30$.

B. Linear potential

As a second example, we consider tunneling through a linear potential barrier

$$V(x) = \theta(x)\left(E_0 x + V_0\right) . \tag{100}$$

The solution of the corresponding Schrödinger equation is given for the domain $x < 0$ by

$$u_1(x, \varepsilon) = e^{ik_1 x} + R e^{-ik_1 x} \tag{101a}$$

with $k_1 = \sqrt{2\varepsilon}$ and the reflection coefficient R. While in the region $x \geq 0$, the solution yields

$$u_2(x, \varepsilon) =$$
$$T\left(\text{Ai}\left(\frac{2E_0 x + 2(V_0 - \varepsilon)}{(2E_0)^{2/3}}\right) + i\,\text{Bi}\left(\frac{2E_0 x + 2(V_0 - \varepsilon)}{(2E_0)^{2/3}}\right)\right)$$
$$= T\,\text{Ai}\left(e^{-2\pi i/3}\frac{2E_0 x + 2(V_0 - \varepsilon)}{(2E_0)^{2/3}}\right), \quad (101b)$$

where Ai and Bi are the Airy function of the first and second kind, respectively. Under the barrier, that is $0 \leq x \leq x_e$ with the tunneling exit point $x_e = -\varepsilon_0/E_0$, the wave function (101b) is a supersposition of reflected and transmitted portions. The transmission coefficient T in (101b) is deduced from matching the wave functions at the border $x = 0$. The phase of the total wave function (101) is used to calculate the Wigner trajectory (83) which is shown in Fig. 14 in comparison with the classical one. This comparison shows that before but close to the tunneling exit x_e a substantial time delay builds up which is reduced after tunneling. Finally, a non-vanishing Wigner time delay remains which is detectable at a remote detector. This time delay is induced at the entering the barrier and equals by magnitude $\tau = 1/(2\sqrt{(V_0 - \epsilon)\epsilon})$.

C. Parabolic potential

As a last example we examine the Wigner time delay for tunneling through a parabolic potential barrier

$$V(x) = \theta(x)\left(-\beta\kappa^4 x^2 + V_0\right), \tag{102}$$

with a dimensionless parameter β. In this case, the exact solution for region $x \geq 0$ is given by

$$u_2(x, \varepsilon) = T\,D\left(-\frac{1}{2} - \frac{i(V_0 - \epsilon)}{\sqrt{2}\sqrt{\beta}\kappa^2}, -(-2)^{3/4} x\beta^{1/4}\kappa\right), \tag{103}$$

with the transmission coefficient T and D denoting parabolic cylinder functions [60]. The Wigner and the classical trajectories for tunneling through the parabolic potential are compared in Fig. 15(a). Qualitatively the Wigner time delay behaves as for the linear potential. In the barrier close to the exit a time delay is built up which is reduced after tunneling and eventually a small non-vanishing Wigner time delay remains.

In analogy to Sec. VI A we add to the parabolic potential (102) a static magnetic field in the region $x > 0$ and investigate the spatial drift due to the magnetic field in the Wigner time delay. Introducing the vector potential $A_z(x) = \theta(x)E_0 x$ this scenario can be described by the Hamiltonian

$$H = \frac{p_x^2}{2} + \frac{[p_z + A_z(x)/c]^2}{2} + V(x). \tag{104}$$

The canonical momentum that maximizes the tunneling probability equals $p_z = -0.15 I_p/c$. The coordinate z as a function of x is shown in Fig. 15(b) for this canonical momentum. As in the case of square potential with magnetic field, the spatial shift between the classical and the Wigner trajectories is small.
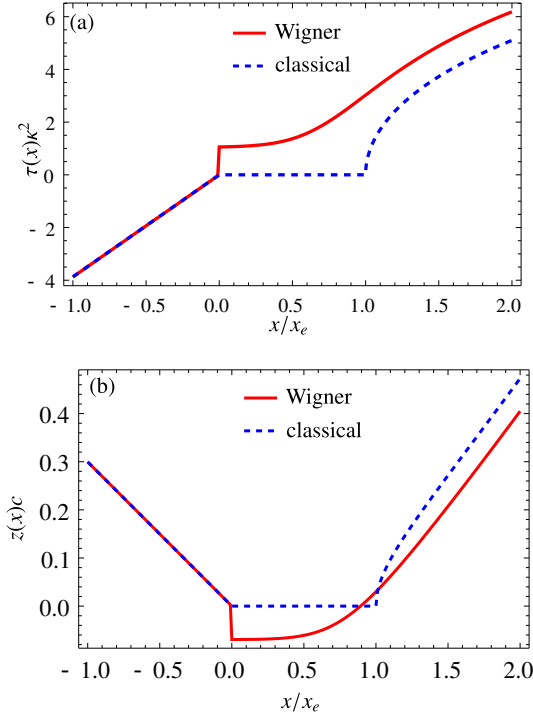
FIG. 15. (Color online) (a) Comparison of the Wigner trajectory (red solid line) and the classical trajectory (blue dashed line) for tunneling through the parabolic potential barrier (102) for $V_0 = \alpha\varepsilon_0$, $\varepsilon_0 = I_p$ with the numerical parameters $\kappa = 90$, $\alpha = 2$ and $\beta = 1/30$. (b) The coordinate z as a function of x for tunneling through a parabolic potential barrier in the presence of a magnetic field.

VII.   TIME DELAY IN TUNNEL-IONIZATION

The previous sections' techniques can be also employed to analyze tunnel-ionization in Hydrogenic ions as considered in Sec. IV. The fundamental difference between the above one-dimensional model systems and tunnel-ionization in Hydrogenic ions is that in the former cases there is a source that produces a positive current incident to the tunneling barrier. In the latter case, however, a bound state tunnels through a barrier and consequently the continuum wave function has to be matched with the bound state wave function (instead of the incident and the reflected plane waves as in the model systems). In the model systems of Sec. VI the Wigner trajectory and the classical trajectory coincide before they enter the tunneling barrier for tunnel-ionization in Hydrogenic ions this is no longer true.

This can be explained by observing that in this case some portion of the bound state always penetrates the barrier. In order to define a meaningful Wigner time delay one has to match the classical trajectory with the Wigner one at the entry point x_0. As a consequence, the Wigner trajectory for tunnel-ionization $\tau_{TI}(x)$ may be defined via the relation

$$\tau_{TI}(x) = \tau(x) - \tau(x_0). \tag{105}$$

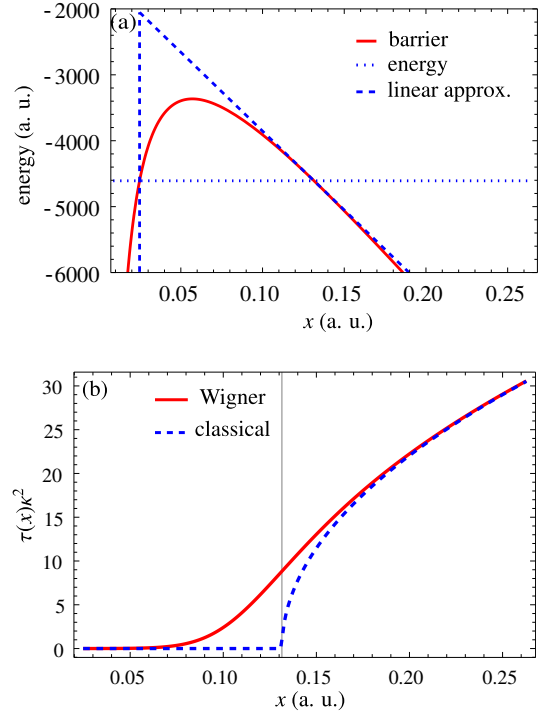Hence the corresponding the Wigner time delay for the tunnel-ionization is identified as

FIG. 16. (Color online) (a) The potential barrier (107) (red solid line) and its linear approximation (109) (blue dashed line) in the deep-tunneling regime. The blue dotted line indicates the energy level of the bound state with $\varepsilon = -Ip$. (b) The Wigner trajectory (red solid line) and the classical trajectory (blue dashed line) in the deep-tunneling regime for nonrelativistic tunnel-ionization with $\kappa = 90$ and $E_0/E_a = 1/30$. Vertical black line indicates the exit coordinate.

$$\tau_W = \tau_c(\infty) - \tau_{TI}(\infty) \tag{106}$$

with the classical trajectory $\tau_c(x)$. Since the coefficients that match the bound wave function and the continuum wave function are position independent the Wigner trajectory $\tau_{TI}(x)$ for tunnel-ionization is solely determined by the phase of the wave function which is the solution of the corresponding Schrödinger equation for the potential

$$V(x) = \theta(x - x_0)(xE_0 - \kappa/x) \tag{107}$$

and represents asymptotically a plane wave. Although, there is no analytical solution for this potential approximate solutions can be found in limiting cases which we will discuss in this section.

A.   Nonrelativistic case

In the one-dimensional tunneling picture, the relevant Schrödinger equation with the electric dipole approximation is given by

$$\left(-\frac{1}{2}\frac{d^2}{dx^2} + xE_0 - \frac{\kappa}{|x|}\right)\psi(x) = \varepsilon\,\psi(x). \tag{108}$$
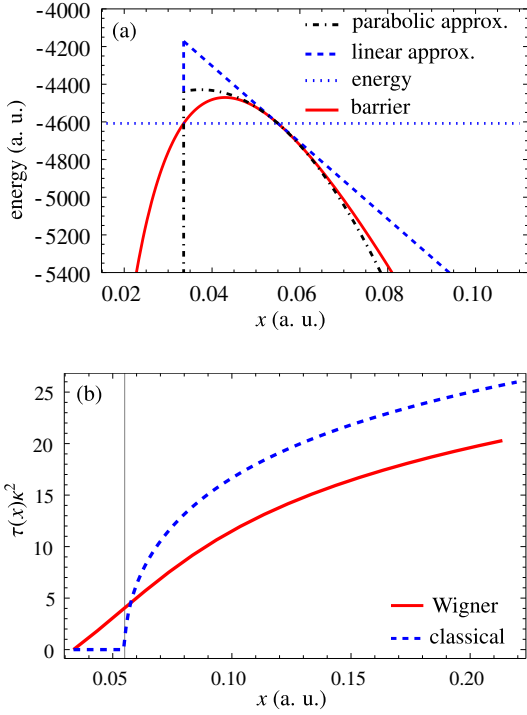
FIG. 17. (Color online) (a) The tunneling barrier (107) (red solid line), its linear approximation (109) (blue dashed line), and the quadratic approximation (111) (black dash-dotted line) in the near-threshold-tunneling regime. The blue dotted line indicates the energy level of the bound state with $\varepsilon = -I_p$. (b) The Wigner (red solid line) and the classical trajectories (blue dashed line) in the near-threshold-tunneling regime for nonrelativistic tunnel-ionization with $\kappa = 90$ and $E_0/E_a = 1/17$. Vertical black line indicates the exit coordinate.

When the tunneling-potential is of sufficient height (deep-tunneling regime) the potential barrier (107) can be approximated near the tunneling exit point x_e by a linear potential

$$V(x) = V(x_e) + V'(x_e)(x - x_e),\qquad (109)$$

see Fig. 16(a). With this approximation the problem of tunnel-ionization in Hydrogenic ions resembles the case of a linear potential as discussed in Sec. VI B. Therefore, in the deep-tunneling regime, the solution of the Schrödinger equation is given by the Airy function

$$\psi(x) = \text{Ai}\left(e^{-2\pi i/3}\frac{-2xV'(x_e) - 2\left(\varepsilon + V(x_e) - x_e V'(x_e)\right)}{2^{2/3}\left(-V'(x_e)\right)^{2/3}}\right).$$
(110)

Note, that the potentials considered in Sec. VI B and here differ in their positions, heights, and slopes. The comparison between the Wigner trajectory and the classical trajectory are plotted in Fig. 16(b). In contrast to the linear potential case of Sec. VI B the Wigner trajectory catches up the classical one at far distance and consequently the Wigner time delay vanishes.

When the electric field strength is increased but the dynamics still remains in the tunneling regime the linear approximation (109) becomes invalid. We may call this regime near-threshold-

tunneling regime of ionization. In this regime the potential may be approximated by including the next quadratic term

$$V(x) = V(x_e) + V'(x_e)(x - x_e) + V''(x_e)\frac{(x - x_e)^2}{2},\quad (111)$$

see Fig. 17(a). As a consequence, the solution of the Schrödinger equation in the near-threshold-tunneling regime is given in the form of parabolic cylinder function as

$$\psi(x) = D(a, b) \qquad (112a)$$

with

$$a = -\frac{i\left(V'(x_e)^2 - \left(2\varepsilon + 2V(x_e) + i\sqrt{V''(x_e)}\right)V''(x_e)\right)}{2V''(x_e)^{3/2}},$$
(112b)

$$b = \frac{(1 - i)\left(V'(x_e) + (x - x_e)V''(x_e)\right)}{V''(x_e)^{3/4}}. \qquad (112c)$$

Comparison of the Wigner and the classical trajectories in the near-threshold-tunneling regime is shown in Fig. 17(b). A non-vanishing Wigner time delay exists in this case due to the parabolic character of the potential barrier near the tunneling exit x_e.

B. Magnetic dipole effects

When the laser's magnetic field is taken into account, tunnel-ionization in Hydrogenic systems can be described by a one-dimensional model if one introduces a position dependent energy level inside the barrier as discussed in Sec. IV. In this one-dimensional model the role of the curvature of the potential barrier and, therefore, its approximations are the same as in the nonrelativistic case within the electric dipole approximation. As for the square and the parabolic potentials with magnetic field we calculate the Wigner time delay when the tunneling probability is maximal. This happens at a certain non-vanishing momentum along the laser propagation direction.

The leading term in $1/c$ is the magnetic dipole correction. Including the latter into the Schrödinger equation in the electric dipole approximation yields

$$\left[-\frac{1}{2}\frac{d^2}{dx^2} + \frac{(p_z - xE_0/c)^2}{2} + xE_0 - \frac{\kappa}{|x|}\right]\psi(\boldsymbol{x}) = \varepsilon\psi(\boldsymbol{x}).$$
(113)

As a consequence of the presence of the vector potential term, for both deep-tunneling and near-threshold-tunneling regimes, the relevant solutions are given by parabolic cylinder functions. Since the quadratic approximation includes also the deep-tunneling regime, in the former case the solution yields

$$\psi(x) = D(a, b) \qquad (114a)$$

with

$$a = \frac{c\left(-cV''(x_e)\sqrt{c^2V''(x_e)+E_0^2}-E_0^2\sqrt{E_0^2/c^2+V''(x_e)}\right)}{2\left(c^2V''(x_e)+E_0^2\right)^{3/2}}$$
$$+\frac{c^3\left(V''(x_e)\left(p_z^2+2V(x_e)-2\epsilon\right)-V'(x_e)^2\right)}{2\left(c^2V''(x_e)+E_0^2\right)^{3/2}}$$
$$+\frac{c\left(-2cE_0p_z\left(V'(x_e)-x_eV''(x_e)\right)\right)}{2\left(c^2V''(x_e)+E_0^2\right)^{3/2}}$$
$$+\frac{c\left(E_0^2\left(x_e^2V''(x_e)-2\left(x_eV'(x_e)+\epsilon\right)+2V(x_e)\right)\right)}{2\left(c^2V''(x_e)+E_0^2\right)^{3/2}}, \quad (114b)$$

$$b = -\frac{i\sqrt{2}\left(c^2(x-x_e)V''(x_e)+c^2V'(x_e)+E_0(cp_z+E_0x)\right)}{c^2\left(E_0^2/c^2+V''(x_e)\right)^{3/4}}.$$
$$(114c)$$

In the deep-tunneling regime, where the potential barrier is approximately linear, the Wigner time delay vanishes as plotted in Fig. 18(a). However, when tunneling happens in the near-threshold-tunneling regime, there exists a non-zero Wigner time delay, see Fig. 18(b). Its order of magnitude equals the result of the nonrelativisitic near-threshold-tunneling regime ionization, compare Figs. 17(b) and 18(b). Moreover, due to the non-vanishing Wigner time delay, a spatial shift between the classical trajectory and the Wigner trajectory along the laser's propagation direction is expected because of the Lorentz force. Both trajectories are shown in Fig. 18(c).

C. Relativistic effects

In order to investigate relativistic effects in the relevant weakly relativistic regime, the leading relativistic corrections to the kinetic energy are expected to be dominant with regard to the Wigner time delay. For simplicity, the exact Klein-Gordon equation is solved where, however, the higher order relativistic effects play no significant role in our scenario. Other leading relativistic effects in $1/c^2$ as those dependent on the spin and on the magnetic field are conjectured to be smaller than the leading relativistic correction to the kinetic energy. In our one-dimensional intuitive picture of Sec. IV, the relevant corresponding Klein-Gordon equation yields

$$\left(-c^2\frac{d^2}{dx^2}+c^4\right)\psi(x)=(\varepsilon-V(x))^2\,\psi(x). \quad (115)$$

with the potential barrier (107).

In the deep-tunneling regime, we can linearize the potential barrier, i.e., $V(x)=V(x_e)+V'(x_e)(x-x_e)$. The corresponding solution which has asymptotically the form of a plane wave reads
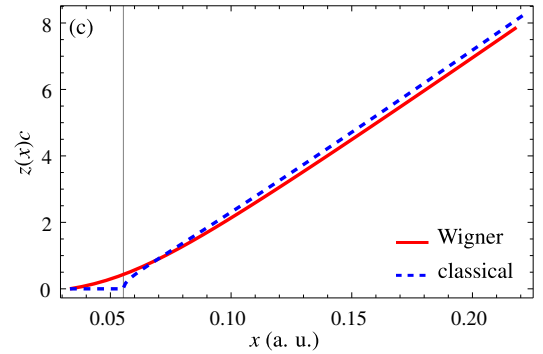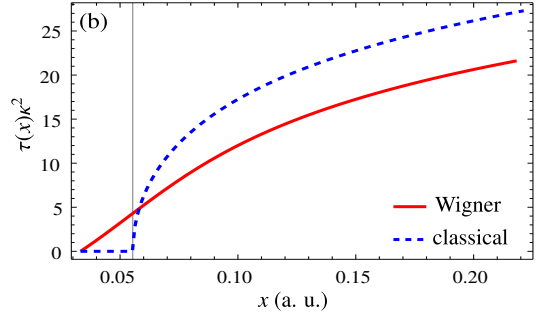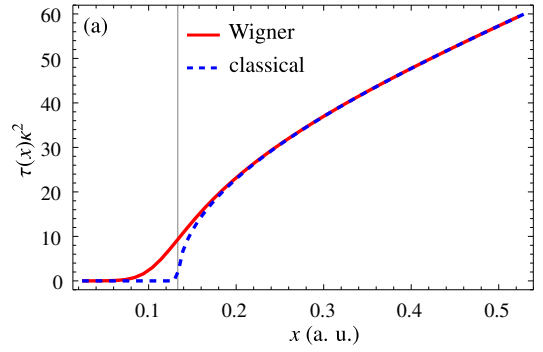
$$\psi(x)=D(a,b) \quad (116a)$$

with

FIG. 18. (Color online) Comparison of the Wigner (red solid line) and the classical trajectories (blue dashed line) for tunnel-ionization taking into account leading effects in $1/c$ (magnetic dipole effects): (a) for the deep-tunneling regime with the most probable momentum at the exit $q_z(x_e)=0.28 I_p/c$, $\kappa=90$ and $E_0/E_a=1/30$; (b) for the near-threshold-tunneling regime with $q_z(x_e)=0.12 I_p/c$, $\kappa=90$ and $E_0/E_a=1/17$. Corresponding classical and Wigner trajectories z as a function of x are presented in sub-figure (c) for parameters of sub-figure (b). Vertical black lines indicate the exit coordinate.

$$a=-\frac{1}{2}+\frac{ic^3}{2V'(x_e)}, \quad (116b)$$

$$b=-\frac{(1+i)\left((x-x_e)V'(x_e)+V(x_e)-\varepsilon\right)}{\sqrt{c}\,\sqrt{V'(x_e)}}. \quad (116c)$$

For the deep-tunneling regime, where the Wigner time delay is zero in the nonrelativistic case, the relativistic corrections to the kinetic energy are also not able to induce a non-zero Wigner time delay as illustrated in Fig. 19.

As pointed out in Sec. VII A an analysis of tunneling from a Coulomb potential in the near-threshold-tunneling regime employs best a quadratic fitting of the tunneling barrier in the vicinity of the tunneling exit. However, there is still no ana-
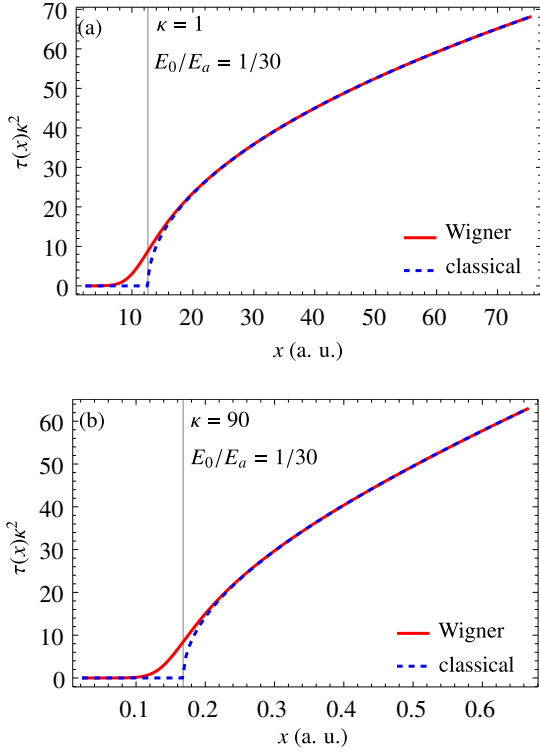
FIG. 19. (Color online) Comparison of the Wigner trajectory (red solid line) and the classical trajectory (blue dashed line) for tunnel ionization taking into account kinematic relativistic effects for the deep-tunneling regime employing nonrelativistic (part (a)) and relativistic (part (b)) parameters. In both parameter regimes no non-zero time delay is detectable at remote distance. Vertical black line indicates the exit coordinate.

lytic solution to this problem. Therefore, we replace now the Coulomb potential again with a zero-range potential rendering the linear approximation applicable again apart for the singular position of the core. Note that the high nonlinearity of the effective potential barrier near the core is still maintained. Then, the solution indicates that the leading relativistic correction to the kinetic energy has a negligible effect on the Wigner time delay as illustrated in Fig. 20. In this figure, the scaled Wigner time delay $\tau_W I_p$ for the nonrelativisitic (dashed lines) as well as relativistic case (solid lines) is shown for different values of I_p and of E_0/E_a.

D. Intuitive explanation of the Wigner time delay

The Wigner time delay and its differing behavior in the deep-tunneling and near-threshold-tunneling regimes can be understood qualitatively as follows. At the introduction of Sec. VII we characterized the Wigner time delay as a deviation of the most probable quantum path from its corresponding classical path at remote distance. Thus, we express the quantum mechanical position and momentum as $x = x_e + \delta x$ and $p = p_e + \delta p$ with x_e and p_e denoting the classical position and momentum at the tunnel exit. When $x_e \gg \delta x$ (as in the deep-tunneling regime), the Wigner time delay vanishes, while
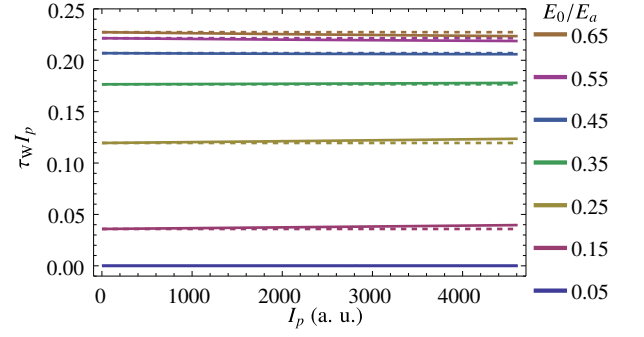

FIG. 20. (Color online) The scaled Wigner time delay $\tau_W I_p$ as a function of I_p for different values of E_0/E_a for tunnel-ionization taking into account relativistic kinematic effects (solid lines) and for nonrelativisitic tunnel-ionization (dashed lines) for the zero-range potential. Note the increasing small deviations of the scaled Wigner time delay with increasing I_p(relativistic effects).

when δx becomes of the order of x_e (as in the near-threshold-tunneling regime) a non-zero Wigner time delay exists.

Considering the Hamiltonian for a nonrelativisitic particle which tunnels trough a potential barrier $V(x)$

$$H = \frac{p^2}{2} + V(x) \tag{117}$$

the corresponding Schrödinger equation in terms of δx and δp follows via inserting above expressions as

$$\frac{\delta p^2}{2} + \delta x \, V'(x_e) = 0 \tag{118}$$

with $V(x_e) = \varepsilon$ and $p_e = 0$. Employing the uncertainty relation $\delta x \delta p \sim 1$, the deviation from the classical trajectory is consequently of the order

$$|\delta x| \sim \left| V'(x_e)^{-1/3} \right| . \tag{119}$$

From this it follows $\delta x/x_e \sim (E_0/E_a)^{2/3}$ for a zero-range potential. Thus the ratio $\delta x/x_e$ grows as ones approaches the near-threshold-tunneling regime and, therefore, a growing Wigner tunneling time delay is expected. This is consistent with our results in Fig. 20. Note that Eq. (119) applies also to the Coulomb potential and we obtain qualitatively the same results.

To sum up, a possible experimental verification of the tunneling time delay is expected to be feasible in the near-threshold-tunneling regime. This delay is approximately proportional to $1/I_p$ as shown in Fig. 20.

VIII. CONCLUSIONS

We have carried out an investigation of the relativistic regime of tunnel-ionization with an emphasis on the role of the under-the-barrier dynamics. In the quasistatic limit, the potential barrier of the relativistic tunneling can be defined in a gauge invariant manner by means of an analysis of the physical energy operator. In contrast to the nonrelativistic case, the relativistic

tunnel-ionization in the quasistatic limit is modeled as tunneling through a potential barrier in an additional magnetic field. Moreover, the latter problem is shown to reduce to one-dimensional tunneling with a coordinate dependent energy.

Later on, using the SFA, we have calculated the momentum distributions of the ionized electron wave packet at the tunnel exit. We showed that the Lorentz force due to the magnetic field during the under-the-barrier motion induces a momentum shift of the electron in the laser propagation direction.

In the second part of the paper, the problem of tunneling time delay has been considered. Although, there is no well-defined time operator in quantum mechanics, it is possible to infer information about the tunneling time delay via tracing the peak of the wave packet, which brings in the so-called Wigner

time concept. The Wigner time formalism was applied to the nonrelativistic as well as to the relativistic tunnel-ionization process. It was shown that the Wigner time formalism can be simplified further for the tunnel-ionization process, due to the fact that the quasiclassical trajectory starts at the entry point of the barrier. In the nonrelativisitic case, it was illustrated that the Wigner time delay vanishes for the deep-tunneling regime when the potential barrier at the tunneling exit can be approximated by its tangent line. At a large laser field strength, in the near-threshold-tunneling regime of the tunnel-ionization, the potential barrier is not linear in coordinate at the tunnel exit. Consequently, the Wigner time delay is preserved at far distances. Finally, our results were extended to the relativistic regime. It was shown that the Wigner time delay is characterized mainly by the nonrelativisitic dynamics.

[1] C. I. Moore, A. Ting, S. J. McNaught, J. Qiu, H. R. Burris, and P. Sprangle, Phys. Rev. Lett. **82**, 1688 (1999).
[2] E. A. Chowdhury, C. P. J. Barty, and B. C. Walker, Phys. Rev. A **63**, 042712 (2001).
[3] M. Dammasch, M. Dörr, U. Eichmann, E. Lenz, and W. Sandner, Phys. Rev. A **64**, 061402 (2001).
[4] K. Yamakawa, Y. Akahane, Y. Fukuda, M. Aoyama, N. Inoue, and H. Ueda, Phys. Rev. A **68** (2003), 10.1103/PhysRevA.68.065403.
[5] E. Gubbini, U. Eichmann, M. Kalashnikov, and W. Sandner, J. Phys. B: At., Mol. Opt. Phys. **38**, L87 (2005).
[6] A. D. DiChiara, I. Ghebregziabher, R. Sauer, J. Waesche, S. Palaniyappan, B. L. Wen, and B. C. Walker, Phys. Rev. Lett. **101**, 173002 (2008).
[7] S. Palaniyappan, R. Mitchell, R. Sauer, I. Ghebregziabher, S. L. White, M. F. Decamp, and B. C. Walker, Phys. Rev. Lett. **100**, 183001 (2008).
[8] A. D. DiChiara, I. Ghebregziabher, J. M. Waesche, T. Stanev, N. Ekanayake, L. R. Barclay, S. J. Wells, A. Watts, M. Videtto, C. A. Mancuso, and B. C. Walker, Phys. Rev. A **81**, 043417 (2010).
[9] V. Yanovsky, V. Chvykov, G. Kalinchenko, P. Rousseau, T. Planchon, T. Matsuoka, A. Maksimchuk, J. Nees, G. Cheriaux, G. Mourou, and K. Krushelnick, Opt. Express **16**, 2109 (2008).
[10] A. Di Piazza, C. Müller, K. Z. Hatsagortsyan, and C. H. Keitel, Rev. Mod. Phys. **84**, 1177 (2012).
[11] W. Becker, F. Grasbon, R. Kopold, D. Milošević, G. G. Paulus, and H. Walther, in *Advances In Atomic, Molecular, and Optical Physics*, Vol. 48, edited by B. Bederson and H. Walther (Academic Press, San Diego, 2002) pp. 35–98.
[12] L. V. Keldysh, Zh. Eksp. Teor. Fiz. **47**, 1945 (1964).
[13] S. Augst, D. Strickland, D. D. Meyerhofer, S. L. Chin, and J. H. Eberly, Phys. Rev. Lett. **63**, 2212 (1989).
[14] P. B. Corkum, Phys. Rev. Lett. **71**, 1994 (1993).
[15] H. R. Reiss, Phys. Rev. Lett. **101**, 043002 (2008).
[16] G. Nimtz, Foundations of Physics **41**, 1193 (2011).
[17] L. A. MacColl, Phys. Rev. **40**, 621 (1932).
[18] L. E. Eisenbud, Ph.D. thesis, Princeton University, Princeton (1948).
[19] E. P. Wigner, Phys. Rev. **98**, 145 (1955).
[20] F. T. Smith, Phys. Rev. **118**, 349 (1960).
[21] R. Landauer and T. Martin, Rev. Mod. Phys. **66**, 217 (1994).
[22] D. Sokolovski, in *Time in Quantum Mechanics*, Lecture Notes in Physics, Vol. 734, edited by J. G. Muga, R. Sala Mayato, and Í. L. Egusquiza (Springer, Berlin, Heidelberg, 2007) pp. 195–233.
[23] A. M. Steinberg, in *Time in Quantum Mechanics*, Lecture Notes in Physics, Vol. 734, edited by J. G. Muga, R. Sala Mayato, and Í. L. Egusquiza (Springer, Berlin, Heidelberg, 2007) pp. 333–353.
[24] Y. Ban, E. Y. Sherman, J. G. Muga, and M. Büttiker, Phys. Rev. A **82**, 062121 (2010).
[25] E. A. Galapon, Phys. Rev. Lett. **108**, 170402 (2012).
[26] P. Eckle, M. Smolarski, P. Schlup, J. Biegert, A. Staudte, M. Schöffler, H. G. Muller, R. Dörner, and U. Keller, Nature Phys. **4**, 565 (2008).
[27] P. Eckle, A. N. Pfeiffer, C. Cirelli, A. Staudte, R. Dorner, H. G. Muller, M. Buttiker, and U. Keller, Science **322**, 1525 (2008).
[28] A. N. Pfeiffer, C. Cirelli, M. Smolarski, D. Dimitrovski, M. Abusamha, L. B. Madsen, and U. Keller, Nature Phys. **8**, 76 (2012).
[29] A. Landsman, M. Weger, J. Maurer, R. Boge, A. Ludwig, S. Heuser, C. Cirelli, L. Gallmann, and U. Keller, "Tunneling time in ultrafast science is real and probabilistic," (2013), arXiv:1301.2766.
[30] M. Klaiber, E. Yakaboylu, H. Bauke, K. Z. Hatsagortsyan, and C. H. Keitel, Phys. Rev. Lett. **110**, 153004 (2013).
[31] A. M. Perelomov and V. S. Popov, Zh. Eksp. Theor. Fiz. **50**, 1393 (1966).
[32] V. S. Popov, Physics-Uspekhi **47**, 855 (2004).
[33] V. S. Popov, Phys. Atom. Nuclei **68**, 686 (2005).
[34] S. V. Popruzhenko, G. G. Paulus, and D. Bauer, Phys. Rev. A **77**, 053409 (2008).
[35] S. Popruzhenko and D. Bauer, J. Mod. Opt. **55**, 2573 (2008).
[36] H. R. Reiss, Phys. Rev. A **42**, 1476 (1990).
[37] H. R. Reiss, J. Opt. Soc. Am. B **7**, 574 (1990).
[38] F. H. M. Faisal, J. Phys. B: At., Mol. Opt. Phys. **6**, L89 (1973).
[39] H. R. Reiss, Phys. Rev. A **22**, 1786 (1980).
[40] M. Klaiber, K. Z. Hatsagortsyan, and C. H. Keitel, Phys. Rev. A **71**, 033408 (2005).
[41] M. Klaiber, E. Yakaboylu, and K. Z. Hatsagortsyan, Phys. Rev. A **87**, 023417 (2013).
[42] R. Mills, Amer. J. Phys. **57**, 493 (1989).
[43] S. Weinberg, *Lectures on Quantum Mechanics* (Cambridge University Press, Cambridge, 2013).
[44] H. Bauke and C. H. Keitel, Comp. Phys. Comm. **182**, 2454 (2011).
[45] The one-dimensional motion along the laser electric field during tunneling ionization can also be justified from the following

estimation. The role of different forces can be evaluated by their contribution to the action, which can be estimated by an order of magnitude as $S \sim \varepsilon\tau$, where ε is the typical energy and τ is the typical time of an acting force. The contribution from the laser electric field is $S_L \sim \tau_K x_e E_0 \sim \kappa^3/E_0 = E_a/E_0$, with the typical distance on which the laser electric field acts on the tunneling electron $x_e \sim \kappa^2/E_0$ (the barrier length) and the Keldysh time τ_K. The contribution from the Coulomb potential can be separated into two parts. The longitudinal Coulomb force contribution is of the order of $S_c^{\parallel} \sim (\kappa/x_c)\tau_c \sim 1$, with the typical time τ_c and coordinate $x_c \sim \kappa\tau_c$, where the Coulomb force makes the main contribution on the electron. The transverse Coulomb force contribution can be estimated via $S_c^{\perp} \sim F_c^{\perp} z_c \tau_c \sim z_c^2/x_c^2 \sim \sqrt{E_0/E_a}$, where the transverse Coulomb force is $F_c^{\perp} \sim \kappa z_c/x_c^3$, the typical longitudinal coordinate is derived equating the laser and Coulomb forces $\kappa/x_c^2 = E$, and the typical transverse coordinate is estimated from $\kappa z_c^2 \sim x_c$. Therefore, the longitudinal contribution of the Coulomb potential into the dynamics represents the leading order correction to the zero-range potential case, while the transversal effect of the Coulomb potential is an higher order correction in the tunneling regime where E_0/κ^3 is small and will be neglected in the following.

[46] The typical value of p_z is already of order of $1/c$ and the $-\hat{p}_z^4/8c^2$ term is neglected as an higher order term in the $1/c$ expansion.

[47] D. M. Wolkow, Z. Phys. **94**, 250 (1935).

[48] E. M. Lifshitz, L. P. Pitaevskii, and V. B. Berestetskii, *Quantum Electrodynamics*, Course of Theoretical Physics, Vol. 4 (Butter-worth Heinemann, Oxford, 1996).

[49] M. Klaiber, E. Yakaboylu, and K. Z. Hatsagortsyan, Phys. Rev. A **87**, 023418 (2013).

[50] M. Klaiber, K. Z. Hatsagortsyan, and C. H. Keitel, Phys. Rev. A **75**, 063413 (2007).

[51] C. T. L. Smeenk, L. Arissian, B. Zhou, A. Mysyrowicz, D. M. Villeneuve, A. Staudte, and P. B. Corkum, Phys. Rev. Lett. **106**, 193002 (2011).

[52] A. S. Titi and G. W. F. Drake, Phys. Rev. A **85**, 041404 (2012).

[53] W. Pauli, *Prinzipien der Quantentheorie I / Principles of Quantum Theory I*, edited by S. Flügge, Handbuch der Physik Encyclopedia of Physics, Vol. V 1 (Springer, Heidelberg, 1958) p. 60.

[54] P. Carruthers and M. M. Nieto, Rev. Mod. Phys. **40**, 411 (1968).

[55] A. I. Baz', Yad. Fiz. **4**, 252 (1966).

[56] A. Peres, Amer. J. Phys. **48**, 552 (1980).

[57] P. C. W. Davies, Amer. J. Phys. **73**, 25 (2005).

[58] E. Merzbacher, *Quantum Mechanics* (John Wiley, New York, 1961) p. 31.

[59] Note that the matching coefficients are found requiring continuity of the wave function $u(x, \varepsilon)$ which includes the reflected portion of the wave function rather than $u_+(x, \varepsilon)$. Furthermore, one can also omit the reflected portion of the wave packet valid for the under-the-barrier motion by setting C_2 zero in Eq. (86). However it does not affect the Wigner time delay.

[60] M. Abramowitz and I. A. Stegun, eds., *Handbook of Mathematical Functions with Formulas, Graphs, and Mathematical Tables* (Dover Publications, Mineola, 1972).